CHAPTER 2

Radiology Case Presentation—General Guidelines

Radiology case presentation guidelines followed by the Stanley Medical College is similar to case presentations in various exams and FRCR Viva. It includes short cases and long cases. These guidelines will aid in the structuring of the radiological report and also its evaluation by the examiners. The report should be succinct and relevant. The examination includes X-ray, CT, ultrasound, radionuclide and MR scans. Candidates will be provided with a double viewing box/monitor, a magnifying glass and a ruler. A brief case history and other relevant clinical data will be provided. Each case may comprise up to four modalities in films or dicom images depending on spotter, short or long case. These vary in complexity and difficulty; some require more time for analysis and reporting than others. It should be ensured that sufficient time is allocated to report each case adequately.

Candidates are expected to start reading the films with a little delay as soon as the films are mounted on the viewing box. There is no need to list dates of investigations or to list all sequences unless these factors are of direct relevance. Similarly, there is no need to repeat the clinical information that has been given, but should use the clinical information in interpreting the observations.

A better performance will be expected in the interpretation of common and routine investigations rather than highly specialised investigations. Examiners mostly will show examples from the major clinical radiology sub-specialties. Candidate's power of observation and deduction will be assessed. A logical and informed approach to film interpretation, as well as a clear ability to debate the merits, relevance and role of further investigative modalities, will be expected. Examiners may ask supplementary questions to assess the understanding of the given clinical problem.

In reaching a conclusion, diagnoses should be given in the order of probability. Long lists regurgitated indiscriminately make it difficult for the faculty to assess the true acumen of candidate. In some cases, the correct diagnosis can be directly arrived at. In others, further views or investigations will be helpful and it is important that the candidate clearly substantiates the reasons for wanting the additional data.

During presentation, the faculty will attempt to assist the candidate to perform to the best of his/her ability. Do not stop the discussion unless the examiner interrupts in between. The candidate has to discuss all the positive findings and points relevant to his/her diagnosis. The candidate should not stop presenting a case unless he does not get the answer for a **"What Next"** question. Listen carefully for any clues provided and must not be afraid to ask for clarification regarding questions asked and doubts regarding the patient's clinical presentation. The examiner will point out any incorrect statements, inappropriate further investigations and management made by the candidate.

The amount of discussion that takes place on each case will vary and is at the discretion of the individual examiner. The actual number of cases shown is immaterial. It is more important that a meaningful dialogue is taking place with the faculty. Patient confidentiality must be respected.

It is strongly advised to follow a standard format (Stanley Medical College Radiology resident reporting format), i.e. approach to **diagnosis first, followed by management and discussion** about the condition (Table 2.1).

Table 2.1: Sample presentation template	
Stanley Medical College—radiology resident presentation template–**what next?**	
1	**Name:** **Age/Sex:** **Occupation:** **Date and time:** **Interval imaging:** **Referred from:** Emergency/OPD/IPD (if relevant and provided)
2	**Clinical presentation:** **Clinical examination:** **Biochemical results:** (if relevant)
3	**Radiological techniques, part in the study, and observations (positive and negative findings, associated findings, complications related to the condition, other organs)** In this section, the candidate should record his/her observations of all the imaging studies available on the films/monitor, including detailed description on positive findings as well as relevant negative findings and brief note on remaining organ systems. Image description of lesion includes site, size, shape, margins, extent, characterisation, skip lesions, nodal involvement/ metastasis and enhancement pattern as appropriate.
4	**Structured analysis and interpretation through logical approach (A-C-B-D-E-F approach)**—there is interpretation of the observed findings which can provide explanation regarding the etiology and complications. For example, description whether lesion being observed is benign or malignant, infective rather than neoplastic, giving your reasons for the same. There is reanalysis with patient data, clinical findings, previous images and biochemical values to arrive at the final diagnosis. **A-C-B-D-E-F approach:** **A**natomy (epicenter) and age **C**haracteristics (size, shape, margins, extents, diffusivity, necrosis, vascularity) **B**ehavior and extension (skip lesions, adjacent organs, enhancement pattern, regional and distal spread) **D**ifferential work up and diagnosis: Substantiate with positive and negative findings. (Further elaborated in the latter part of the section) The steps A-C-B-D should happen in the Radiologist's thought process (Not a part of Reporting template) **E**valuation further and **F**ollow-up imaging
5	**Principal diagnosis (substantiate with positive and negative findings):** Based on the candidate's interpretation he/she should attempt to come to a single diagnosis especially in cases where the findings are classical (e.g. tuberous sclerosis). **Relevant differential diagnosis—balance of probability:** In classical cases, there is no differential diagnosis. If the case is complex, then he should state which diagnosis he/she feels is most likely and then list other possibilities in order of likelihood, in the differential diagnosis section which should be limited to relevant 2–3 conditions. However, in this book we have also added some rarer differential diagnosis for the purpose of elaborate discussion and to enlighten students.
6	**Management (recommended further investigations—treatment goals)/applied radiology in treatment** A. *Critical cases*–immediately inform the referring/appropriate clinician (e.g. acute infarct, EDH with brain herniation, pulmonary embolism, encephalitis, pneumothorax, cardiac tamponade, pseudoaneurysm, acute abdomen) B. *Noncritical cases:* Relevant further investigations—laboratory, radiological and nuclear medicine, HPE (reasons for wanting additional data) to confirm the diagnosis. C. *For tumours:* Confirmatory HPE examinations followed by local and locoregional staging by MRI/CT scan. PET scan for systemic staging. Treatment depends on the stages/cellular type of disease. Final decision on treatment is based on discussion in multidisciplinary tumour board. Similarly, if the candidate makes a diagnosis of an abscess or tumour, he should indicate if a drainage or biopsy is appropriate.
7	**Brief discussion about the condition in viva:** Here the candidate should discuss about the diagnosis of his case and briefly discuss the etiopathology, clinical presentation, treatment options and some note on differential diagnoses.

SPECIMEN REPORTS

Case 1: A six months old child seen unconscious in the emergency department.

Case history: Age—6 months/female child

Clinical presentation: Unconscious/no history of trauma.

Radiological Techniques and Observations

1. Non-contrast CT scan brain (Fig. 2.1)
2. X-ray chest (Fig. 2.2)/X-ray thigh (Fig. 2.3)/X-ray knee (Fig. 2.4)

Observations (*see* Figs 2.1 to 2.4)**:** A non-contrast head CT shows chronic subdural hematoma in bilateral frontal convexity and new subdural haemorrhage in right frontal convexity and posterior interhemispheric SDH. Minimal midline shift is seen to the left side. No skull fracture is seen on these images. X-ray thigh AP view shows displaced spiral midshaft fracture in right femur. X-ray left knee shows corner fracture in upper end of tibia. Chest X-ray shows fractures of the right first to eighth ribs in posterior aspect with evidence of callus formation indicating healing. There are also fractures of the left fourth to ninth ribs posteriorly but no associated

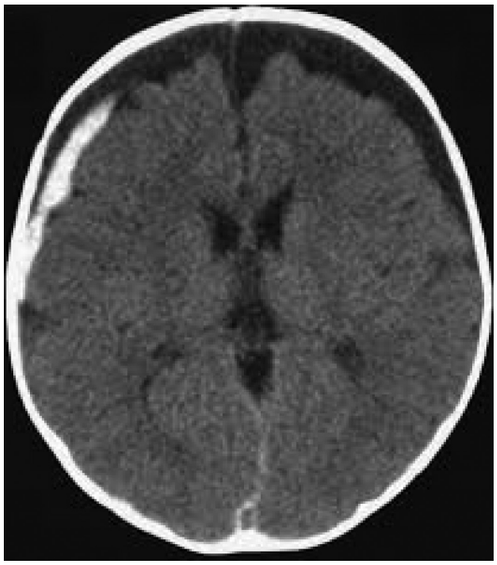

Fig. 2.1

Fig. 2.2

Fig. 2.3

Fig. 2.4

callus or periosteal new bone, suggesting that these fractures have occurred very recently. The lung fields are clear.

Analysis and Interpretation

CT brain: Extra axial fluid collection lies within the sub-dural rather than the sub-arachnoid space. It contains both high and low attenuation material indicating that it is likely to represent an acute or chronic sub-dural haematoma.

Chest X-ray: Shows multiple rib fractures in different stages of healing.

X-ray thigh: Spiral midshaft fracture in right femur

X-ray knee: Corner fracture in upper end of left tibia.

Principal diagnosis: Non-accidental trauma, since the fractures are at different stages of healing and some new fractures also seen and acute on chronic subdural hematoma in brain in absence of skull fracture adds to the diagnosis of non-accidental trauma.

Differential diagnosis: Consider accidental trauma. This appears unlikely in view of the posterior rib fractures of different ages.

Management: The patient needs an urgent neurosurgical opinion and the child protection service must be alerted. A skeletal survey should be performed to look for other fractures and to ensure that there is no evidence of any other skeletal abnormality, such as osteogenesis imperfecta.

Brief discussion about the condition: Non-accidental trauma is a complex injury in infants and young children as a result of abuse. Diagnosis of non-accidental trauma has direct impact on medical, social and legal outcomes of children and families. The classical metaphyseal corner or bucket handle fracture is virtually pathognomonic for abuse. Lateral and posterior rib fractures are highly specific for abuse. Patterns of skull fracture that suggest child abuse are multiple 'eggshell' fractures, occipital impression fractures, fractures crossing sutures. CNS injury especially subdural hematoma is common in child abuse. Visceral injuries include liver, pancreatic laceration and adrenal bleeding are specific for child abuse.

Case 2: A 12 months old child with abdominal distension and seizure.

Case history: 12 months/male child

Clinical presentation: Complaints of abdominal distension for 2 months with 1 episode of seizure.

Radiological investigations and observations: CT brain, MRI brain and CT abdomen.

Observations on CT brain (Fig. 2.5)**:** Hyperdense extra-axial mass lesion noted in right fronto-parietal convexity and left parietal convexity.

Observations on MRI brain (Fig. 2.6): TI post-contrast image shows heterogeneously enhancing extra-axial dural mass noted in bilateral parietal convexity.

Observations on CECT abdomen (Fig. 2.7): Large heterogeneous mass soft-tissue dense mass in left suprarenal fossa extending into midline with coarse stippled calcifications.

Analysis and Interpretation

CT/MRI brain: Diffuse dural mass lesion involving bilateral parietal and right frontal convexity in a 12 months old child.

CT abdomen: Soft-tissue mass in left suprarenal fossa with coarse stippled **calcifications,** this is likely to relate to a malignancy in the adrenal gland.

Principal diagnosis: Neuroblastoma in left adrenal region with cranial metastasis as my printcipal diagnosis considering the age of the child.

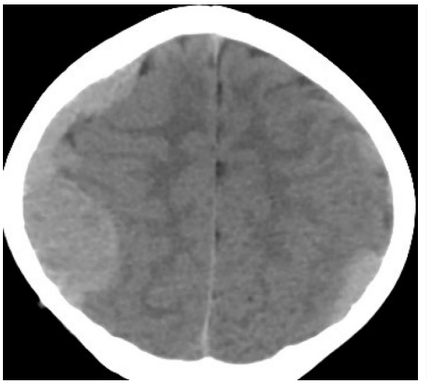

Fig. 2.5

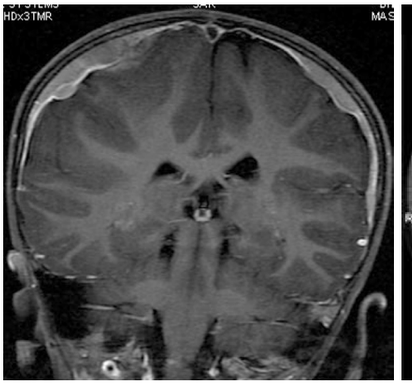

Fig. 2.6

Fig. 2.7

Differential diagnosis: Adrenal carcinoma can rarely occur in this age group and may calcify but is unlikely to extend intraspinally. Wilms' tumor is intrarenal, only occasionally calcifies and rarely metastases to bone so should not give these appearances.

Management: **Further investigations required**—ultrasound, MRI, bone/MIBG scan, PET.

An ultrasound scan would confirm whether the calcified mass lies within the adrenal gland.

Bone scan/I^{131} MIBG scan: Nuclear scintigraphy with areas of increased activity suggests skeletal metastases. An MRI scan and PET scan would be required for staging and monitoring response to treatment. Bone marrow aspiration and catecholamine estimation are usually also performed. A biopsy may also be required.

Brief discussion about the condition: Neuroblastomas are tumors of neuroblastic origin. They represent the most common extracranial solid childhood malignancy. Common metastatic sites are bone, liver, lung, pleura and brain.

SAMPLE REPORTING TEMPLATES

There is no specific standardized reporting template available, here we provided some sample pathological reporting templates used in our department, and reporting templates need constant revision based on recent updates.

Central Nervous System

Arachnoid cyst: Left anterior temporal arachnoid cyst compressing adjacent anterior and medial temporal lobe with adjacent bony scalloping. It measures 40 (TR) × 39 (CC) × 47 (AP) mm. It elevates and displace left middle cerebral artery medially. There is significant mass effect on the left lateral ventricle with midline shift to right (7 mm)—Galassi type-III.

Medulloblastoma: Evidence of well-defined large heterogeneously enhancing mass lesion measuring about 3.5 × 4.5 × 5.3 cm (AP × TR × CC) arising from the vermis (roof of fourth ventricle) within the 4th ventricle causing moderate obstructive hydrocephalus and transependymal seepage of CSF and cerebellar tonsil herniating 6 mm below the foramen magnum. Fourth ventricle CSF is seen anteriorly as cleft. There is significant compression on the brain stem. No intra-axial edema. The lesion is highly cellular showing T2 hypo/isointense signal with restricted diffusion, areas of necrosis and calcifications. MR spectroscopy shows reduction of NAA, elevation of choline, elevated lipid lactate peak and taurine peak. Entire neuraxis imaging shows no leptomeningeal enhancement or drop metastasis. Mass is extending into the foramen of Luschka on left side and foramen of Magendie (in cases of ependymoma)–medulloblastoma–group 4.

Ectopic posterior pituitary gland: Ectopic posterior pituitary gland along the median eminence of hypothalamus with absent pituitary stalk. Thin anterior pituitary—hypoplastic.

Choroidal fissural cyst: Choroidal fissural cyst measuring about 15 × 7 mm causing mild mass effect over the left hippocampus.

High grade glioma: 2.8 (TRANS) × 5.7 (AP) × 3.6 (CC) cm size hypointense lesion in T1w, hyperintense in T2W sequences seen at the peritrigonal, left parieto-occipital lobe compressing the trigone and posterior horn of left lateral ventricles. There is surrounding perilesional oedema extending to the left optic tract. The lesion extending along the splenium of corpus callosum to the right peritrigonal parietal white matter. It shows peripheral diffusion restriction. There is mild midline shift to the right (5.6 mm). The lesion shows increased vascularity with areas of hemorrhage. MR spectroscopy shows significant elevation of choline, lactate and lipid. On contrast administration the lesion shows heterogeneous enhancement with increased regional CBF and CBV in perfusion imaging. On tractography no significant reduction in the density of the corticospinal tracts and other white matter fibers. Left arcuate fibers are compressed and displaced medially. On finger tapping in the right hand, cortical activation was observed along the superior and lateral aspect of left precentral gyrus. The lesion is well away from the hand motor area.

On word generation (language) fMRI, activation noted in left inferior frontal gyrus and left superior temporal gyrus, left supramarginal gyrus along antero-superolateral aspect of the lesion and parietal opercula anterior to the lesion. Minimal activation also noted in the right supramarginal gyrus and right angular gyrus.

Low grade glioma: Well-defined heterogeneous mass lesion in the left supramarginal gyrus, left angular gyrus and indenting on the posterosuperior aspect of left superior temporal gyrus. The lesion shows areas of hemorrhage. No evidence of mass effect/prominent arterial feeder/contrast enhancement. MR spectroscopy shows mild elevation of choline, lactate and lipid.

DNET: Well-defined T2 hyperintense lobulated expansile, cortical based 42 mm (AP) × 35 mm (transverse) × 38 mm (craniocaudal) size lesion in the left frontal parasagittal region (left paracentral lobule) with facilitated diffusion and partial suppression in FLAIR. No evidence of

surrounding perilesional vasogenic oedema/mid-line shift. On spectroscopy the lesion shows elevated choline, lactate and decreased NAA. No evidence of any other T2/FLAIR grey matter hyperintensity. Above MR features favours dysembryoplastic neuroepithelial tumor (DNET) than low grade glioma.

Functional MRI: Activation of right motor cortex (right precentral gyrus) observed, during finger tapping with left hand. On finger tapping with right hand, cortical activation was observed along the superior and medial aspect of left precentral gyrus and adjacent paracentral lobule and also along the posterior rim of the left paracentral lobule lesion. On bilateral finger tapping, bilateral motor cortex, supplementary motor cortex activation was noted (left > right). No evidence of plasticity.

Tractography: Shows displacement of the corticospinal tract posteriorly. No evidence of infiltration/destruction of corticospinal tract. Corticobulbar fibres are displaced anteriorly and inferiorly. A few posterior fibres were destroyed. Superior longitudinal fasciculus is displaced laterally. Superior fronto-occipital fasciculus appears normal.

Atypical teratoid rhabdoid (ATRT): Evidence of large solid and cystic mass lesion measuring about 7.1 × 6.4 × 7.5 cm (AP × TR × CC) in left side of posterior fossa with significant mass effect over the cerebellum and brainstem. Enhancing solid nodules with hemorrhagic areas seen along the medial aspect of mass. There is compression and narrowing of the 4th ventricle and aqueduct with moderate obstructive triventricular hydrocephalus and periventricular seepage of CSF. Mass is pushing the brainstem and cerebellum to right side. No extension to IAC. Superomedially cystic component is extending up to the pineal region/posterior 3rd ventricular region. Features favour the possibility of atypical teratoid rhabdoid tumor (ATRT) in left side posterior fossa with significant mass effect.

Brainstem glioma: 29 × 28 × 27 mm (AP × TR × CC) size expansile exophytic lesion in the left side of pontomedullary junction and left middle cerebellar peduncle with areas of hemorrhage in the inferior aspect. There is expansion of left middle cerebellar peduncle with compression on the left side of fourth ventricle. There is significant surrounding edema in the medulla, left cerebellum, bilateral thalamus and posterior capsular regions. MR spectroscopy shows marked elevation of choline, marked reduction of NAA peak and presence of lactate. Features favour brainstem glioma. DTI shows displacement of pontocerebellar fibers laterally and corticospinal tract fibres medially. Mass effect noted in the left corticospinal tract without significant white matter loss. Leptomeningeal enhancement seen in/around the spinal cord in the cervicodorsolumbar region—**suggestive of drop metastasis.**

Pineoblastoma: 22 mm (AP) × 19 mm (TR) × 23 mm (CC) size well-defined heterogeneously enhancing lobulated mass lesion with peripherally dispersed calcification in the pineal region extending to the upper part of the aqueduct with areas of haemorrhage causing dilatation of third and lateral ventricles. Tectal plate and suprasellar region appear intact. No evidence of leptomeningeal metastasis. On spectroscopy the lesion shows mildly elevated choline and decrease NAA. The lesion shows diffusion restriction—above features favours pineoblastoma than germinoma.

***Choroid plexus papilloma*:** Large T2 heterogeneous mass with frond-like pattern in the trigone of left lateral ventricle. It measures 6.8 × 4.8 × 6.7 cm. No demonstrable calcification or hemorrhage is seen at present. Both lateral, third and fourth ventricle are dilated. No evidence of acute infarct. Mild midline shift to the right measuring 4 mm. There is moderate dilation of right lateral ventricle and gross dilatation of left lateral ventricle. The lesion shows homogeneous enhancement with cauliflower-like appearance. No obvious evidence of intraparenchymal extension/parenchymal edema. There is prominent arterial supply from the lateral posterior choroidal artery, anterior choroidal artery and the prominent choroidal vein drains into the thalamostriate vein. No obvious evidence of leptomeningeal/drop metastasis. MR spectroscopy shows elevated choline significantly decreased NAA and creatine.

Hypothalamic hamartoma: Well-defined non-enhancing T1 hypointense long TR mild hyperintense lesion in the tuber cinereum/hypothalamus region causing partial narrowing of the third ventricle and abutting the optic tract. MR spectroscopy of the lesion shows mildly decreased NAA peak.

Diffuse cerebral atrophy (children)—Grey matter neurodegeneration: GM gangliosidosis and neuronal ceroid lipofuscinosis. Suggested clinical/biochemical correlation. Other possibilities include: Glycogen storage disorder. Mucolipidosis, multiple sulfatase deficiency, post-encephalitis sequelae.

Cerebellar atrophy (children): Moderate to severe cerebellar atrophy with ex-vacuo dilatation of 4th ventricle. FLAIR hyperintense cerebellar cortex (INAD, Marinesco-Sjögren, late onset GM2 gangliosidosis, late infantile NCL).

Moderate to severe **cerebral and cerebellar atrophy** with increased T2W signal intensity in the white

matter and excess iron deposition in the basal ganglia. Possibilities include: Neuro degeneration with brain iron accumulation–pantothenate kinase associated neurodegeneration (Hallervorden-Spatz disease), oculodigital dental dysplasia, Kufor-Rakeb syndrome (pallidopyramidal degeneration), neuronal ceroid lipofuscinosis, glycogen storage disease.

Severe cerebellar atrophy (children): Severe cerebellar atrophy with T2W/FLAIR increased cerebellar cortex signal intensity. Evidence of flat pons. Clava hypertrophy noted. No evidence of basal ganglia atrophy/basal ganglia T2 hyperintensity/supratentorial hypomyelination. Mild increased iron deposition in globus pallidus. MR spectroscopy of the brain parenchyma shows normal spectral pattern. No significant reduction of NAA/elevation of choline. No abnormal metabolites seen. Possibilities include: Infantile neuraxonal dystrophy, congenital disorder of glycosylation (Pmm2-CDG)—no evidence of flat pons seen, Marinesco-Sjögren SIL1, ceroid lipofuscinosis (late), juvenile GM2 (late).

Arteriovenous malformation (AVM): Abnormal cluster of vessels (arteriovenous malformation nidus) measuring about 27 × 19 mm in the inferolateral aspect of the left inferior parietal gyrus in the angular gyrus and adjacent parieto-occipital region. No acute hemorrhage/surrounding edema. No obvious evidence of infarct/atrophy. Lesion is fed by cortical branches of left MCA and left PCA. Venous drainage to superior sagittal sinus. No adjacent gliosis. Spetzler-Martin grade-I.

Aneurysm: 7.3 × 6 × 8.5 mm size multilobulated saccular aneurysm seen arising from the M1 bifurcation of right middle cerebral artery/anterior communicating artery. The aneurysm is arising from the posterior aspect and pointing posterosuperiorly. Neck of the aneurysm measures 2.3 mm. No obvious evidence of any other aneurysm, wall irregularity/thrombus/vasospasm/subarachnoid hemorrhage/infarct/bleb/lobulation.

Giant cavernous malformation: 37 (TR) × 22 (AP) × 28 (CC) mm size T2W multilobulated lesion in the right inferior frontal gyrus, frontal central white matter extending near the anterior body of right lateral ventricle with minimal surrounding oedema. It shows hyperintense signal with popcorn appearance. The lesion blooms in SWI sequence in the periphery. Mild midline shift to left (2 mm). No obvious dilated feeding artery/draining vein seen. Multiple cavernomas—**familial multiple cavernous malformation syndrome.**

Developmental venous anomaly: Abnormal dilated venous channels draining into the collector subependymal vein in the right frontal region.

Molar tooth malformation—Joubert syndrome: Abnormal configuration of the midbrain with typical "molar tooth" appearance. Enlarged 4th ventricle with "bat-wing" configuration and enlarged cisterna magna. Absent cerebellar primary fissure and fastigial point. Hypoplasia of the vermis with apposition (not fusion) of cerebellar hemispheres and clefting of the superior cerebellar vermis. High riding 4th ventricle with deep pontomesencephalic junction.

Dorsal tegmental tract hyperintensity: Abnormal T2W/FLAIR hyperintensity in the midbrain and upper pons and dorsal tegmental tract—usually seen in cerebral palsy.

Creatine deficiency syndromes: Minimal hyperintensity noted in the dentate nucleus, medial portion of middle cerebellar peduncle and nucleus accumbens. MR spectroscopy of the brain shows markedly decreased creatine—**creatine deficiency syndromes** can be considered (guanidinoacetate methyltransferase (GAMT) deficiency, deficiency of L-arginine: Glycine amidinotransferase (AGAT), defect in a creatine transporter protein).

Parecho virus encephalitis: Evidence of restricted diffusion in bilateral frontoparietal and temporal subcortical white matter and corpus callosum. Punctate T1W hyperintensities seen in bilateral frontoparietal subcortical white matter. MR spectroscopy of the brain parenchyma shows normal spectral pattern. No abnormal metabolites seen. Features favour the possibility of Parecho virus/dengue/chikungunya encephalitis.

Craniosynostosis: Altered shape of the skull. Premature fusion of bilateral coronal suture leading to craniosynostosis with increased convolutional markings in the frontal bone (anterior plagiocephaly). Increased convolutional markings secondary to craniosynostosis. Sagittal, metopic, lambdoid and squamosal sutures are normal.

Microcephaly: Microcephaly with simplified gyral pattern in frontal and temporal region.

CT Cisternogram: **CSF leak:** 1.6 × 3.2 mm size bony defect in the left cribrifrom plate of ethmoid bone with CSF leak into the left nasal cavity.

Pontine tegmental cap dysplasia: Abnormal brainstem with hypoplastic pons and flattened ventral surface. Shrunken cerebellum and focal bulging of the pontine tegmentum projecting into the fourth ventricle—pontine tegmental cap dysplasia.

Hippocampal malrotation/vertical hippocampus/hippocampal inversion: Vertical orientation and medial

positioning of head and body of left hippocampus with round hippocampal head—hippocampal malrotation, above features show association with malformations of cortical development and temporal lobe epilepsy.

van der Knaap disease (megalencephalic leukoencephalopathy with subcortical cysts): Diffuse T2 W and FLAIR hyperintensities, not showing restricted diffusion in bilateral cerebral deep and subcortical white matter and external capsule. Multiple subcortical cysts in bilateral temporal lobes and high frontal regions.

Metachromatic leukodystrophy: Confluent bilateral symmetrical periventricular white matter hyperintensity with gliosis and mild ex-vacuo dilatation of both lateral ventricles. Bilateral symmetrical white matter hyperintensity also involves subcortical U fibers, external capsule, posterior limb of internal capsule, dorsal aspect of pons, middle cerebellar peduncles and bilateral cerebellar white matter.

Metachromatic leukodystrophy (early changes): Confluent periventricular white matter hyperintensities on T2 W/FLAIR sequence with no significant restricted diffusion. Both thalami and basal ganglia are preserved. No significant involvement of brainstem/subcortical U fibers. MRS shows mild reduction of NAA, rise in choline with no significant changes in other metabolite peaks.

Krabbe disease: Diffuse T2 W/Flair hyperintensity involving the periventricular, subcortical cerebral white matter, internal capsule, corpus callosum, dorsal brain stem, deep cerebellar white matter with high myelin edema. T2 hypointense signal noted in the bilateral thalamus which is hyperdense in CT. MR spectroscopy shows no significant abnormal metabolite—above features favour Krabbe disease. Suggested clinical/lab parameter correlation.

Hypomyelination: Severe hypomyelination/demyelination (myelination of only perirolandic white matter and central white matter).

Hypomyelination/leukodystrophy with diffuse thinning of corpus callosum: Possibilities include: 1. Hypomyelinating leukodystrophy–III, 2. hypomyelination and congenital cataract, 3. HSP60 chapernopathy, 4. Salla disease.

Canavan's disease: Bilateral cerebral subcortical and periventricular white matter, internal capsule, external capsule, globus pallidus, dentate nucleus, extreme capsule, cerebral peduncle, dentate nucleus, dorsal brainstem, deep cerebellar white matter shows T2W diffuse hyperintensities and hypointense in T1W FLAIR images. These changes appear bright in diffusion weighted images. Caudate and putamen appear normal. On spectroscopy, the lesion shows increased NAA compounds. Suggested urinary and plasma N-Aspartyl acetic acid/clinical correlation.

Alexander disease: T2W/FLAIR hyperintensity in the bilateral frontal, temporal white matter, external capsule, extreme capsule, basal ganglia, thalamus, brainstem and periventricular white matter garlands in the peritrigonal occipital region without diffusion restriction. On contrast administration mild enhancement noted along the ventricular lining and periventricular white matter in the frontal white matter. On spectroscopy, the lesion shows mildly decreased NAA peak.

Glutaric aciduria type I: Arachnoid cyst in bilateral anterior temporal regions (middle cranial fossa) with hypoplasia of the underlying temporal lobes—Bat wing shape with widened sylvian fissures. Hyperintensity involving caudate and lentiform nucleus, white matter, dorsal brain stem with diffusion restriction.

Anterior temporal pole cyst with calcification: Leukoencephalopathy with calcifications and cysts (LCC), TORCH (congenital CMV infection)/pseudo-TORCH (Aicardi–Goutières syndrome), cystic leukoencephalopathy without megalencephaly (RNASET 2-deficient cystic leukoencephalopathy), Cockaye syndrome (no basal ganglia calcification/cerebral atrophy).

Anterior temporal pole cyst without calcification: Abnormal T2W/FLAIR hyperintensities in bilateral peritrigonal and perilateral white matter, which does not show diffusion restriction. Bilateral anterior temporal pole cyst seen. No obvious evidence of basal ganglia and cerebral calcification seen. MR spectroscopy of the brain parenchyma shows normal spectral pattern. No significant reduction of NAA/elevation of choline. No abnormal metabolites seen. Possibilities include, TORCH (congenital CMV infection)/pseudo-TORCH (Aicardi–Goutières syndrome)—no evidence of calcification seen. Megaloencephalic leucoencephalopathy with subcortical cysts (no obvious megalencephaly). Leukoencephalopathy with calcifications and cyst—no evidence of calcification seen. Congenital muscular dystrophy.

Excessive T2W hyperintense changes noted in the bilateral deep white matter region. No evidence of PVL. No abnormal diffusion restriction. Diffuse and excessive high signal intensity (DEHSI)—**suggestive of normal finding in preterm infant. Mild elevated lactate peak—normal for age.**

Hypoglycemic (hypoxic) ischemic brain injury sequelae: Bilateral parieto-occipital gliosis with ex-vacuo dilatation of occipital horn of lateral ventricles.

***Hypoxic ischemic encephalopathy* (HIE):** Diffuse bilateral periventricular white matter hyperintensity

with white matter loss, ex-vacuo dilatation of both lateral ventricles with undulated margins. Mild diffuse thinning of the corpus callosum. Features favour the possibility of **periventricular leucomalacia** (hypoxic ischemic encephalopathy).

Abnormal T2W/FLAIR hyperintensity in the bilateral thalamus and posterior putamen—**profound hypoxic ischemic brain injury sequelae.**

Diffusion restricting T2 hypointense lesion seen throughout the cerebral parenchyma involving the deep grey matter and thalamus. Diffusion restricting lesion noted in the entire corpus callosum and internal capsule and extension along the corticospinal tract. Cerebellum and posterior brainstem relatively appear normal. MR spectroscopy of the brain parenchyma shows significantly elevated lactate peak seen throughout the brain parenchyma. **Features are suggestive of severe hypoxic ischemic encephalopathy changes.**

T2W hyperintensity in bilateral posterior lentiform nucleus, thalami, perirolandic frontoparietal regions, bilateral periventricular and deep white matter. Diffuse thinning of corpus callosum. Mild ex-vacuo dilatation of both lateral ventricles. MR spectroscopy shows reduction of NAA and presence of lactate in affected areas: **Features are suggestive of sequelae of perinatal hypoxic ischemic encephalopathy.**

Gliosis in left frontal, temporal, parietal and occipital cortex and white matter with ex-vacuo dilatation of left lateral ventricle, secondary hypoplasia of brainstem on left side and reduced volume of skull. Milder gliosis in right frontal and parietal cortex and white matter. Features are suggestive of sequelae of hypoxic ischemic encephalopathy (**multicystic encephalomalacia).**

Benign enlargement of subarachnoid space: Prominent bilateral frontotemporal arachnoid spaces—benign enlargement of subarachnoid spaces (normal variant). **Or** Widening of bifrontal subarachnoid spaces (cranio-cortical diameter >5 mm)—suggestive of benign physiologic enlargement of subarachnoid spaces (otherwise known as benign macrocephaly of infancy/external hydrocephalus/physiologic extraventricular obstructive hydrocephalus). It is a self-limited condition with spontaneous resolution of CSF spaces between 12–24 months.

Iron deposition (children): Abnormal T2W/FLAIR hyperintensity in the caudate nucleus, anterior aspect of putamen with bilateral globus pallidus. MR spectroscopy of the basal ganglia shows decreased NAA and mildly increased lactate. Bilateral optic atrophy. Moderate to severe atrophy of cerebellum and pons. Mild diffuse cerebral atrophy. Above feature favour metabolic/neuro degeneration. Possibilities include: Mitochondrial disorder/fatty acid associated neurodegeneration suggested clinical/lab parameter correlation.

Methylmalonic acidemia: Bilateral symmetric altered signal intensity appearing hypointense on T1W and hyperintense on T2W noted in globus pallidus without diffusion restriction/contrast enhancement. MR spectroscopy shows no significant abnormal metabolite. Possibilities include: Methylmalonic Acidemia, Kernicterus (less likely—no history of neonatal jaundice), Succinate semialdehyde dehydrogenase deficiency, L-2-hydroxy glutaric aciduria, isovaleric acidemia, neonatal hypoxia.

Bilateral putaminal T2W/FLAIR hyperintensity (putaminal necrosis): With diffusion hyperintensity and elevated lactate in MR spectroscopy. SWI shows no increased iron deposition. Possibilities include: Mitochondrial disease—including G14459A mutation, SUCLA-2 gene mutation. Pediatric autoimmune neuropsychiatric disorder associated with streptococcal infection (PANDAS). Propionic academia. Neuroacanthocytosis—additional features like cerebellar atrophy is absent. No evidence of thalamus, midbrain, pons involvement to suggest Wilson disease. No evidence of T1 hyperintensity in globus pallidus. Methanol intoxication/hypoxic ischemic changes—no supportive clinical history. Juvenile Huntington's disease—no evidence of caudate nucleus involvement. Molybdenum cofactor deficiency—no evidence of caudate nucleus, white matter involvement. Glutaric aciduria—no other white matter/bilateral sylvian arachnoid cyst **(refer to case 4.28).**

Bilateral globus pallidus T2W/FLAIR hyperintensity (adult): Bilateral globus pallidus T2W/FLAIR hyperintensity with diffusion restriction—possibilities include: 1. Poisoning (carbon monoxide), 2. Hypoglycemia/hypoxia, 3. Cocaine/heroine abuse. Neuro degeneration with brain iron accumulation less likely.

Caudate and putamen: Abnormal T2W/FLAIR/diffusion weighted hyperintensities in the caudate and putamen. MR spectroscopy shows elevated lactate—features favours Leigh's disease. Other possibilities include: Propionic academia, molybdenum cofactor deficiency, Wilson's disease, juvenile Huntington's disease, osmotic myelinolysis, hemolytic uremic syndrome, hypoxia—less likely, carbon monoxide poisoning **(refer to case 4.27).**

Prominent Virchow-Robin spaces: In bilateral cerebral hemisphere—possibilities include Lowe syndrome, mucopolysachridoses, hypomelanosis of Ito and velocardiofacial syndrome.

Bilateral thalamus without haemorrhage: Non-diffusion restricting long TR hyperintense lesions noted in the both

thalamus, bilateral outer putamen and caudate nucleus and bilateral patchy supratentorial subcortical and deep white matter and pons, midbrain central white matter. Possibilities include: Japanese encephalitis. Cerebral malaria/acute disseminated encephalomyelitis (rare).

Bilateral thalamus with haemorrhage: Bilateral thalamic hyperintensities with/without diffusion restriction and haemorrhages. Normal deep venous system noted. Possibilities to be considered: Flavi virus encephalitis like Japanese encephalitis, cerebral malaria, H3N2 influenza encephalitis with vasculitis (acute necrotizing encephalitis), herpes simplex encephalitis (no involvement of temporal lobe in this patient), dengue fever (haemorrhage less likely).

Reversible splenial lesion: Focal lesion in the splenium of corpus callosum which shows diffusion restriction without hemorrhage—reversible splenial lesion syndrome (RESLES) probably due to encephalitis/encephalopathy of varied etiology.

Tubulinopathy: Diffuse thinning of corpus callosum. Thin anterior commissure. Irregular prominent bilateral lateral ventricles—moderate ventriculomegaly. Enlarged caudate nucleus and fused striatum (absent diminutive internal capsule dividing the caudate from putamen): Dysmorphic basal ganglia—above features favour tubulinopathy (DYNC1H1 mutation).

Arnold-Chiari malformation Type 1: Small posterior fossa with cerebellar tonsilar herniation 8 mm below the foramen magnum line causing crowding of the foramen magnum. Evidence of syringomyelia in the cervical cord from C2 to C5 vertebrae level—Arnold-Chiari malformation Type 1. CSF flow shows pulsatile flow in the syringomyelia. No flow noted in the posterior subarachnoid space. Anterior cervical subarachnoid space and pre-pontine and pre-medullary cisterns show normal CSF flow.

Posterior fossa is smaller than normal. Herniation of the cerebellar tonsil below the foramen magnum up to the lower C2 level. 4th ventricle is elongated and slit-like with moderate triventricular hydrocephalus. There is medullary kink, beaking of tectum, large massa intermedia, scalloped posterior petrous pyramids and clivus, large funnel-shaped foramen magnum. Cerebellum wraps around the medulla. Low lying tentorium and torcula.

Pantothenate kinase associated neurodegeneration (Hallervorden-Spatz disease): Mild diffuse cerebral and cerebellar atrophy with increased signal intensity in the globus pallidus giving eye of the tiger appearance. Bilateral basal ganglia calcification seen. MR spectroscopy shows no abnormal metabolite seen. No evidence of altered signal intensity in the cerebellum. Possibilities include: Neurodegeneration with brain iron accumulation—pantothenate kinase associated neurodegeneration (Hallervorden-Spatz disease). Kearns-Sayre syndrome and other mitochondrial disorder NARP (neuropathy, ataxia and retitis pigmentosa).

Table 2.2: MR parkinsonism index-2 (MRPI 2)

	AP diameter	*Width*	*Volume (mm^3)*	*Interpretation*
Midbrain	14 mm			
Superior colliculus	3 mm			
Midbrain (midline) M			1.17	
Pons (midline) P			5.46	
Pons /midbrain area ratio P/M			5.46/1.17 = 4.67	
Superior cerebellar peduncle in coronal plane SCP		4.8 mm		
Middle cerebellar peduncle in sagittal plane MCP		11.1 mm		
MCP/SCP ratio			2.31	
MRI parkinsonism index = (P/M) × (MCP/SCP)		10.79		PSP >13.55
Third ventricular width (V3): Average width (from three measurements) of the 3rd ventricle on axial image at the level of anterior and posterior commissures	9.5 mm			
Frontal horn (FH) (maximal left to right frontal horn width on axial image in AC-PC plane)		37.7 mm		
MRPI 2.0 = MRPI × (V3/FH)		10.79 × 0.251 = 2.70		PSP-P ≥2.18 PSP-R ≥2.5 PD <2

Fukuyama's congenital muscular dystrophy: Cerebellar hypoplasia noted with tiny cortical cysts. Pontine hypoplasia with Z-shaped deformity. Bilateral lissencephaly with cortical polymicrogyria. Periventricular white matter long TR hyperintense lesion. Absent septum pellusidum noted. Bilateral lateral ventricles dilatation. Thickened tectal plate noted. Basal ganglia and thalamus appear normal.

Progressive supranuclear palsy: Diffuse cerebral and cerebellar atrophy. Disproportionate atrophy of midbrain. AP diameter of midbrain measures 11.9 mm, width of middle cerebellar peduncle 6.6 mm, width of superior cerebellar peduncle 1.7 mm on right side and 2.7 mm on left side. Area of midbrain measures 0.68 sq. cm and area of pons measures 3.4 sq cm.

Pituitary macroadenoma: Dumbbell-shaped well-defined enhancing mass lesion with cystic areas of size 36 (CC) × 26 (AP) × 28 (Trans) mm in the sella-suprasellar region compressing and elevating the distal intracranial optic nerves and optic chiasma. Expansion of sella noted. There is extension to right cavernous sinus, reaching up to the lateral venous compartment. Cavernous segment of right internal carotid artery is mildly pushed laterally without stenosis. Sphenoid sinus is well pneumatised. Normal pituitary gland and infundibulum are not made out separately. Tubercinerium, mamillary body, floor of the IIIrd ventricle are normal: Features are suggestive of pituitary macroadenoma. Post-sellar pneumatisation of the sphenoid sinus with prominent sellae bulge and plannum sphenoidale, dorsum sella pneumatisation. Sphenoid sinus show single midline septum anteriorly and multiple septae posteriorly. Inter-carotid distance—20 mm. Optic chiasma is seen over the pituitary and dorsal sellae—normal/post-fixed chiasma.

Viral encephalitis: Diffusion restricting long TR hyperintense lesion in the both putamen, right thalamus, right posterior parietal cortex and right inferior frontal gyri and right amygdala. Possible viral encephalitis.

Rasmussen's encephalitis: Diffuse gyral thickening and T2 hyperintensity noted involving the left cerebral hemisphere (left temporal, frontal and parietal regions). T2 hyperintensity noted in the left thalamus and caudate part of left basal ganglia and left substantia nigra. Focal T2 hyperintensity noted in the subcortical region with left frontal region. No evidence of restricted diffusion. Mass effect noted on the left cerebral sulci and left lateral ventricle with mild effacement. Mild midline shift to right of 2.0 mm noted. Mild leptomeningeal enhancement noted in the left cerebral hemisphere. The different diagnoses are Rasmussen's encephalitis/viral encephalitis/postictal change associated with status epilepticus.

Acoustic schwannoma: Evidence of a large heterointense extra-axial avidly enhancing mass lesion measuring 5.2 (AP) × 3.6 (TR) × 4.1 (CC) cm noted in the left CP angle region. There is extension into the left internal auditory meatus with intrameatal component measuring 5.1 × 5 mm. Distal 3.4 mm of the internal auditory canal appear normal. Fundus of internal auditory canal and cochlear aperture appear normal. Areas of multiple microhaemorrhages within the mass. The lesion is highly vascular with multiple feeders from the left vertebral artery which is hypoplastic. Left VII-VIII nerve complex in the CP angle cistern and proximal IAM are not visualised separately from the mass. There is compression of the pons, lower midbrain, left middle cerebellar peduncle and adjacent cerebellar hemisphere without intra-axial edema. Effacement of aqueduct and fourth ventricle with early obstructive hydrocephalus (dilatation of third and both lateral ventricles). Increased intracranial tension with bilateral prominent perioptic CSF sheath and tortuous optic nerves, flattening of posterior sclera and partial empty sella. Evidence of tonsillar herniation of 12 mm below the foramen magnum.

Eosinophilic granuloma: Evidence of well-defined lytic lesion in the right parietal bone measuring 37 mm (AP) × 15 mm (TR) × 53 mm (CC) with extra-axial and subgaleal soft tissue components. There is destruction of both inner and outer tables. The lesion intracranially abuts the dura which is thickened and demonstrates increased enhancement. No other calvarial lesions are seen. No definite intra-axial abnormality. The infundibulum and cavernous sinuses have a normal appearance.

Tuberous sclerosis: Multiple subependymal nodules along the lateral ventricles predominantly along the caudothalamic groove, cortical tubers in the left postcentral gyrus and right superior frontal gyrus. No evidence of subependymal giant cell astrocytoma/ocular lesions/white matter changes/vascular lesions.

PRES (posterior reversible encephalopathy syndrome): Bilateral frontoparietal, parietal, occipital and left cerebellar subcortical and cortical T2W FLAIR hyperintensity with/without diffusion restriction.

Colloid cyst: Well-defined T1 hyperintense lesion measuring 12.5 mm (AP) × 10.5 mm (TR) × 10 mm (CC) in anterior third ventricle at the foramen of Monro, more towards left side causing mild asymmetric prominence of left lateral ventricle.

Normal pressure hydrocephalus: Age related diffuse cerebral atrophy with prominent cortical sulci and both

lateral ventricles. There is mild disproportionate dilatation of both lateral ventricles compared to sulcal prominence with minimal periventricular hyperintensity along the frontal and occipital horns of both lateral ventricles. Accentuated flow void noted across the aqueduct and adjacent posterior third ventricular region and proximal 4th ventricle. MR spectroscopy of the ventricle shows lactate peak—finding favouring the possibility of normal pressure hydrocephalus over other dementia. No dilatation of IIIrd and IVth ventricle. No ballooning of optic and infundibular recess of third ventricle. No disproportionate dilatation of sylvian fissure.

Alzheimer's disease: Cerebral sulcal spaces, basal cisterns, cerebellar foliae and ventricular system appear prominent. Suggestive of moderate diffuse parenchymal atrophy. Global cortical atrophy scale: score 2. The hippocampus volumes measures 1.30 cm^3 on right side and 1.29 cm^3 on left side—decreased. MTA-scale for Medial Temporal lobe Atrophy: score 3. The interuncal distance at the level of anterior commissure is 31 mm—more than 30 mm is considered as abnormal.

Wilson disease: Bilateral symmetrical FLAIR/T2 hyperintensities in the putamen, thalami, pallidum and tegmentum of midbrain and periaqueductal grey matter. T1 hyperintensity noted in the globius pallidus. Midbrain lesion shows characteristic 'face of the giant panda'—Wilson disease.

Tolosa-Hunt syndrome: Ill-defined hypointense lesion in the right orbital apex and right cavernous sinus, which shows homogeneous enhancement. The lesion measures 20 (AP) × 10 (CC) × 6 (TR) mm. No obvious evidence of dural tail.

Aberrant course of the right anterior inferior cerebellar artery indenting on the right facial nerve at the root entry zone with mild deviation of 7th nerve course. No evidence of **neurovascular conflict at the nerve root entry zone** of left trigeminal nerve.

Mesial temporal sclerosis: Body of the right hippocampus appears small with loss of internal architecture (striations) and loss of hippocampal digitation with increased signal intensity and dilated temporal horn of right lateral ventricle. Right fornix and mamillary body atrophy—right mesial temporal sclerosis. Right hippocampus volume ~1.89 cc. Left hippocampus volume ~2.09 cc.

Acute intracerebral hemorrhage: [60 mm (AP) × 39 mm (TR) × 38 mm (CC)] in the left para sagittal frontal region inter-hemispheric fissure and adjacent sulcal spaces. There is extension to all ventricle more in the left lateral ventricle. Significant mass effect on left lateral ventricle with midline shift to the right (14 mm) anterior body of the corpus callosum is displaced downwards. Mildly prominent right lateral ventricle. Haemorrhage also noted in the sylvian fissure and basal cisterns.

Extra dural haemorrhage: Maximum thickness measuring 18 mm in the left lateral convexity along the parietotemporal region, causing midmass effect with local sulcal effacement and midline shift of 4 mm to the right. No evidence of hydrocephalus. Basal cisterns appears normal. Linear undisplaced Fracture noted in the squamous part of left temporal bone.

Comment about space of the haemorrhage, size, intraventricular extension, obstructive hydrocephalus, edema, midline shift, herniation, any area of infarction, vessel injury, old gliosis, if any.

Small vessel ischemic changes: Multiple focal discrete and confluence T2W/FLAIR hyperintensities in the periventricular and central white matter which does not show diffusion restriction—small vessel ischemic changes. Fazekas scale for WM lesions—score 2.

Acute disseminated encephalomyelitis (ADEM): Altered signal intensity appearing hyperintense on T2 and FLAIR, not showing restriction of diffusion in bilateral basal ganglia, thalamus, brain stem and deep cerebellar white matter. No abnormal enhancement on contrast administration—features favours acute disseminated encephalomyelitis (ADEM).

Acute infarct in the left middle frontal gyrus, inferior frontal gyrus, pre central gyrus, postcentral gyrus, left centrum semiovale, left superior, inferior parietal gyrus, insula, head of left caudate nucleus, left temporoparietal region. Minimal haemorrhagic transformation in the left parietal region. No evidence of significant mass effect**.**

Demyelination: Abnormal T2W/FLAIR hyperintensity in the right superior cerebellar subcortical white matter which does not show diffusion restriction/contrast enhancement—demyelination.

Vasculitis/chronic demyelination plaque: Multiple small T2W and FLAIR hyperintensities, not showing restricted diffusion seen scattered in bilateral fronto parietal subcortical white matter and parieto-occipital periventricular white matter. Normal callososeptal interface. No evidence of Dawson's fingers. No evidence of haemorrhage. No optic nerve demyelination.

Multiple sclerosis: Multiple nondiffusion restricting nonenhancing linear, ovoid and globular long TR hypointensity lesions involving the callososeptal interface, perilateral ventricular regions, bilateral frontal, temporal, parietal, subcortical regions and right internal capsule, left cerebellar white matter, superior cerebellar

Table 2.3: Neuroimaging radiological interpretation system (NIRIS)		
Category	*Definition*	*Patient management/actions*
NIRIS 0	No abnormal finding	Discharge from the ED
NIRIS 1	Fracture ±	Follow-up neuroimaging and/or admit for observation.
	Extra-axial hematoma, intraparenchymal hematoma/contusion <0.5 mL±	
	Subarachnoid haemorrhage.	
NIRIS 2	Extra-axial hematoma, intraparenchymal hematoma/contusion >0.5 mL±	Admit to a more advanced care unit.
	Diffusion axonal injury ±	
	Intraventricular haemorrhage ±	
	Mild hydrocephalus ±	
	Midline shift 0–5 mm	
NIRIS 3	Extra-axial hematoma, intraparenchymal hematoma/contusion >5 mL±	Consider neurosurgical procedure (ventricular drain, burr hole, craniotomy/ craniectomy, surgical drainage/evacuation of hematoma)
	Moderate hydrocephalus ±	
	Midline shift >5 mm ±	
	Focal herniation	
NIRIS 4	Extra-axial hematoma, intraparenchymal hematoma/contusion >25 mL±	High risk traumatic brain injury-related death
	Severe hydrocephalus ±	
	Diffuse herniation/duret haemorrhage	

vermis, pons—right middle cerebellar peduncle junction. Multiple patchy focal lesions in the entire spinal cord involving lateral, central and posterior columns at variable levels. Features favour multiple sclerosis—suggested clinical/CSF of analysis correlation. **Restricted diffusion noted in bilateral central part of the centrum semiovale more on the right side. Patchy peripheral diffusion restriction in the left centrum semiovale lesions (Table 2.4).**

Bilateral T1 hyperintensity in globus pallidus: Bilateral T1 hyperintensity in globus pallidus—possible basal ganglia calcification/hepatocellular—renal dysfunction, manganese deposition (in patients with chronic renal disease on hemodialysis).

Idiopathic intracranial hypertension: Partial empty sella seen. Prominent bilateral perioptic sheath fluid with posterior scleral flattening. Moderate luminal narrowing in bilateral distal transverse sinuses.

Hydrocephalus with post-op status: Post-operative burr hole defect in the frontal and right parietal bone. Moderate dilatation of third and both lateral ventricles with collapsed fourth ventricle–obstructive hydrocephalus. VP shunt tube *in situ* one through the right parieto-occipital and other through the right

Table 2.4: Multiple sclerosis sample reporting						
Region	*Location*	*No of lesions*	*Size*	*Diffusion restriction (+/–)*	*Contrast enhancement (+/-) type of enhancement*	*Comparison with previous MRI New lesions/T1 Black Holes*
Periventricular and callososeptal interface						
Juxtacortical/ cortical						
Infratentorial						
Spinal cord						
Lobar-vloume						Volume loss
Corpus callosum-volume						
Other findings (optic nerc)						

frontal lobe with tip in the body of right lateral ventricle. Bifronto-temporal encephalomalacic gliosis. Paucity of subcortical white matter in the frontotemporal region. Right parieto-occipital loculated fluid collection measuring 46 × 18 mm along the shunt tract near the reservoir.

Head and Neck

CA tongue: 19 (AP) × 10 (TR) × 18 (CC) mm size ill-defined mass lesion in the right anterolateral border of the anterior third of tongue with minimal infiltration of the intrinsic muscles. Mylohyoid, hyoglossus and genioglossus, stylopharyngeus appears normal. No evidence of extension into the mandible/retromolar trigone/lingual septum/floor of mouth/midline/posterior third of tongue—features suggestive of carcinoma tongue. **(T2M0N0)**.

Ca tongue reporting checklist: **Laterality**: **Right or left, Size: ….× …. × … cm.** Depth of invasion: (Previous Depth of invasion:)

T Stage: To comment on whether the tumor crosses the midline or abuts lingual raphe, involvement of extrinsic muscles like genioglossus, hyoglossus, geniohyoid, involvement of lingual neurovascular bundle (grade: 0/I/II/III) and uni/bilateral involvement.

To comment on whether the tumor extends to posterior one-third of the tongue, RMT, tonsillo-lingual sulcus and tonsil extension of tumor to sublingual space/submandibular space, infiltration of mylohyoid and involvement of floor of mouth, comment on extension to masticator space, infratemporal fossa (ITF), high infratemporal fossa. Inferior extent: Look up to vallecular/epiglottis/PFS, also comment on involvement of hyoid, if not involved—comment on distance from hyoid bone. Look for any bony erosion—mandibular involvement, cortical breach, marrow signal abnormality.

N: Presence of nodal disease: Metastatic/benign (reactive)/indeterminate, if indeterminate/suspicious: Need for additional imaging, laterality: Ipsilateral/contralateral/bilateral levels: Level: IA and IB/II, III, IV, V, VI and retropharyngeal. Size of the largest node: Right side: ….. mm and level, Left side: ….. mm and level, presence of necrosis if any, perinodal extension/extracapsular spread: Absent/present, vascular involvement by the nodes: IJV: involved/compressed; CCA, ICA, ECA abutment: Absent/ Present, If present angle of contact for CCA and ICA: <90, 90–179, 180–269; >270. Strap muscles involvement, Prevertebral fascia invasion. M: Lung, hepatic, adrenal and skeletal metastasis.

Juvenile nasopharyngeal angiofibroma (JNA): Large well-defined lobulated highly vascular enhancing mass lesion measuring about 5 × 4.1 × 4.4 cm (AP × TR × CC) noted in the right spheno palatine foramen, posterior nasal cavity, posterior ethmoidal sinus and right sphenoid sinus. Lesion is highly vascular with multiple flow voids within. Main arterial supply of the mass is seen from the hypertrophied right internal maxillary artery. There is widening of the right pterygopalatine fossa and extension of the soft tissue into the infratemporal fossa. Erosion of the medial and lateral pterygoid plate on right side. There is involvement of right foramen rotundum and vidian canal. There is erosion of the anterior wall of the foramen ovale. Erosion of floor of right middle cranial fossa (greater wing of sphenoid) without intracranial extension. No involvement of the ICA. There is extension into the inferior aspect of the orbital apex on right side through the widened inferior orbital fissure. No involvement of the extraocular muscles/optic nerve. Nasal septum is pushed to left. The mass is extending into the nasopharynx—features are consistent with juvenile nasopharyngeal angiofibroma–stage IIc: (staging system proposed by Sessions, modified by Radkowski).

Multi nodular goiter: Thyroid appears diffusely enlarged showing heterogeneous enhancement, right lobe measures ……left lobe measures …….with mild mass effect over trachea, no retrosternal extension of thyroid lobes noted. No significant cervical lymph nodes noted. TIRADS-II.

Post-cricoid carcinoma: An ill-defined soft tissue dense lesion measuring 2 × 1 cm noted in post-cricoid region at the level of C5–C6, the lesion does not extend to bilateral pyriform fossa, the lesion appears to erode cricoid and cricoarytenoid joint, arytenoid appears sclerosed, the lesion infiltrates posterior aspect of larynx with marked narrowing of airways, lesion appears to involve the anterior wall of proximal cervical esophagus for a length of 1 cm causing luminal narrowing of esophagus, recurrent laryngeal nerve appears normal. The parapharyngeal fat planes are infiltrated, no cervical lymphadenopathy.

Glottic growth: Ill-defined soft tissue density lesion measuring about 19 × 11 mm in the right vocal cord. No subglottic extension of the lesion. Minimal infiltration of the right supraglottic fat. No obvious extra laryngeal extension. There is sclerosis of the right arytenoid cartilage - ? Infiltrated.

Supraglottic growth: Soft tissue density lesion measuring about 2.2 × 1.5 cm in the right side of the larynx involving

Table 2.5: Lymphoma reporting tool			
No.	Size (mm) (long-axis diameter) × (short-axis diameter)	FDG uptake (SUVmax)	Location (lymph node location/location within the affected organ)
1.			
2.			

the supraglottic and glottic space. No subglottic extension. There is mild sclerosis of the right aretynoid cartilage and thickening of the right aryepiglottic fold. No involvement of the left vocal cord. A few small subcentimetric lymph nodes in bilateral cervical region.

Lymphoma: Multiple lobulated enlarged lymph nodes noted in the bilateral preauricular, cervical infra-clavicular, hilar, mediastinal lymph nodes. There is no evidence of splenomegaly. With PET scan avid uptake **(SUV 3.0)** noted in the lymph nodes and in the right iliac bone (recommended site for biopsy). No evidence of other lesions in the stomach, liver, lung/pleura, kidney, CNS and skin (Table 2.5).

Vocal cord palsy: Paramedian position of the right vocal cord. Prominent right pyriform sinus with thickened aryepiglottic fold—right vocal cord palsy. No obvious mass lesion in the neck/visualised mediastinum.

***Post-radiation status of larynx*:** Partially abducted left vocal cord with mild effacement of left pyriform fossa and vallecula with thickened (17 × 9 × 17 mm) false cord, supraglottic and glottic region extending to involving the posterior aspect of the pharynx with narrowing of laryngeal inlet. Diffuse non-enhancing edema of the pyriform fossa, Aryepiglottic folds and post-cricoid pharynx. Mild irregularity in the right lateral border of tongue-radiation induced changes

***Vagal schwannoma*:** Evidence of a large extraaxial intra and extracranial dumb bell-shaped heterointense enhancing mass lesion with cystic areas and hemorrhage noted in left jugular foramen, cerebello medullary cistern and CP angle. Extracranially, lesion extends to the upper carotid space. Intracranial component measures 3.9 (AP) × 2.8 (trans) × 3.4 (CC) cm, the component in jugular foramen measures 2 × 1.2 cm, extracranial component in upper carotid space measures 4.5 (trans) × 2.69 (AP) × 3.9 (CC) cm. The left internal carotid artery is displaced anteromedially by the mass and internal jugular vein is compressed posterolaterally and not visualised in the region the mass in carotid space. Medulla and left middle cerebellar peduncle are indented by the mass. No intra-axial edema. No obstructive hydrocephalus. Smooth widening of left jugular foramen. No extension to internal auditory meatus. No extension to hypoglossal canal. Left vocal cord palsy changes seen.

Branchial fistula: 6 mm length linear fistulous tract extending from skin in the left paramedian lower neck extending up to the sternocleidomastoid muscle. No evidence of extension into the left lobe of thyroid/pyriform fossa.

***Lower cranial nerve/jugular schwannoma*:** Large intra- and extra-cranial dumb bell-shaped heterointense enhancing mass lesion with cystic areas and hemorrhage in left upper carotid space, jugular foramen, cerebello medullary cistern and CP angle.

Suppurative lymphadenitis: Conglomerate enlarged left upper and mid cervical lymph nodes and upper posterior triangle lymph nodes with areas of necrosis. No evidence of vertebral, bone or deep neck space involvement.

Carotid body tumor: Well-defined intensely enhancing highly vascular soft tissue density mass lesion measuring 3.6 × 3.7 × 5.2 cm (AP × TR × CC) in the left carotid space at CCA bifurcation level with splaying of the internal carotid and external carotid arteries. The lesion shows salt and pepper appearance in T1/T2 images. Mass is extending superomedially to lower para pharyngeal space. Left internal jugular vein is compressed and pushed laterally without thrombus. There is no encasement of ICA and ECA. No e/o luminal narrowing/thrombus formation. Multiple arterial feeders seen arising directly from proximal external carotid artery, ascending pharyngeal artery and occipital artery. No supply from the ICA.

Chronic otomastoiditis without cholestatoma: Soft tissue noted filling the right middle ear cavity, right external auditory canal, mastoid antrum and mastoid air cells. Soft tissue noted in right facial nerve recess and sinus

Table 2.6: Cochlear implant workup on HRCT	
1	Mastoid cellularity—non-pneumatised / hypo/ normal
2	Middle ear cavity—ossicles integrity and round window
3	Position of genu and descending mastoid segment of facial nerve—any aberrant course
4	Jugular bulb (if high riding)
5	Bony labyrinth structure with special focus on cochlea size, turns, interscalar septum, modiolus, cochlear aperture, cochlear duct length
6	Internal auditory canal
7	Cochlear and vestibular aqueduct

Table 2.7: Cochlear implant workup in MRI	
Signal of fluid in labyrinth	(Hypointense in case of labyrinthitis): Balkany classification of labyrinthitis
Inner ear structures with special focus on cochlea. Scalar anatomy, osseous spiral lamina, outlines of modiolus, cochlear aperture size	Inner ear anomalies
Internal auditory canal with 7–8th nerve complex evaluation	Absence of 8th nerve/ undivided 8th nerve, hyoplastic 8th nerve
Lateral bulbopontine and cerebellopontine angle	For evaluation of any mass lesion
Brain stem (fascicular segment of 8th nerve, cochlear nerve nuclei)	For evaluation of any mass lesion in brain stem
Fascicular segment of 8th nerve-course along lateral aspect of pons, cochlear nuclei-hypointense structure along dorsolateral aspect of inferior cerebellar peduncle	
Auditory pathway and brain survey	Any lesion/ hypoxic changes, demyelination in superior olivary nucleus, lateral leminiscus, medial geniculate body, superior temporal gyrus, Heschl gyrus

Table 2.8: Cochlear implantation work up (measurements)		
Cochlea	2.5–2.75 turns, 29.5–32 mm in length, 8–10 mm height	Cochlear anomalies—aplasia/ hypoplasia
Cochlear aperture	Length: 0.8-1.2 mm, diameter: 1.8–2.5 mm	Diameter <1.4 mm—indicative of cochlear nerve deficiency
Cochlear duct length	CDL = (4.16 * A) – 3.98, A: Largest distance from round window to the lateral wall of cochlea	Electrode array of optimal length to be chosen
IAC diameter		<2.5 mm—absent/ hypoplastic 8th nerve
Cochlear aqueduct		>3 mm—dilated, risk of transmission of ear infection to meninges
Vestibular aqueduct	At midpoint between crus and external aperture	>1.5 mm/calibre is more than half of posterior semicircular canal

Table 2.9: CT reporting and staging system of acquired cholesteatoma		
Tympanic cavity involvement (T)	*Mastoid cavity involvement (M)*	*Complications (C)*
T1: Attic cholesteatoma	M0: No mastoid cavity involvement	C0: Uncomplicated cholesteatoma
T2: Tympanic cholesteatoma	M1: Cholesteatoma extending into mastoid antrum	C1: Temporal complications
T3: Attico-tympanic cholesteatoma	M2: Cholesteatoma extending to mastoid cavity and cells	C2: Cranial and intracranial complications
T4: Holotympanic cholesteatoma		

tympani. No evidence of erosion of scutum/widening of Prussak's space, erosion of malleus and incus on both sides. No erosion of tegmen tympani, lateral semicircular canal or facial nerve canal/sinus plate/inner ear.

Chronic left otomastoiditis with cholesteatoma: Soft tissue noted filling the left middle ear cavity, mastoid antrum and mastoid air cells. Soft tissue noted in left facial nerve recess and sinus tympani. There is erosion of scutum, malleus, incus with widening of Prussak's space. Middle ear soft tissue component measures 12 × 9 mm with extension of soft tissue into the left external auditory canal. No erosion of tegmen tympani, lateral semicircular canal or facial nerve canal/sinus plate/inner ear. No evidence of widening/block of left eustachian tube. Partial sclerosis of left mastoid air cells. No obvious evidence of jugular vein, left sigmoid sinus thrombosis. No obvious evidence of intracranial abscess/ meningeal component. Nonecho planar diffusion shows restricted diffusion.

Temporomandibular joint: Abnormal anterior displacement of articular disc of left temporomandibular joint with inter position of the posterior band between the condyle and the eminence. It remains anteriorly displaced at all times during jaw opening—**anterior displacement without reduction.**

Abnormal anterior displacement of articular disc of right temporomandibular joint with interposition of the posterior band between the condyle and the eminence. It reduces during jaw opening. **Anterior displacement with reduction.**

Right temporomandibular joint articular disc posterior band is located at 12 o' clock position related to condyle in closed mouth and 'bowtie' appearance in between articular eminence and condylar head in open mouth—**normal**.

***Obstructive sleep apnoea in dynamic sleep MRI*:** Severe dynamic airway narrowing with complete obliteration of the lumen at the naso-oropharyngeal junction due to apposition of the posterior margin of the soft plate and the posterior pharyngeal wall during sleep.

Eagle's syndrome: Mildly elongated bilateral styloid process (36 mm in length).

Sinonasalpolyposis: Extensive polypoidal mucosal thickening completely filling the left maxillary, ethmoid, frontal and sphenoid sinuses and nasal cavity. OMU complex is completely blocked on left side. There is extension of the polyp into the nasopharynx through the choana. There is mild sclerosis of the walls of the sinuses—secondary to chronic inflammation. Small mucosal polyp in the right maxillary sinus. Deviation of the nasal septum to right, mild mucosal thickening in right frontal, ethmoid and sphenoidal sinuses. DD: Allergic fungal sinusitis

Sinusitis: Minimal mucosal thickening in left maxillary sinus. Kero's type I skull base. Bilateral partial concha bullosa. Hypertrophy of both inferior turbinate.

Os terminale–Os odontoideum: Hypoplastic dens with wide gap between the os terminale–os odontoideum complex, which is seen near the basi occiput (dystrophic). Enlarged anterior arch of atlas. Evidence of atlanto-axial instability along with prominent retro os odontoideum soft tissue causing myelomalacic changes in the cervical cord at C1–C2 vertebrae level.

Anteriorly displaced C2 body and posteriorly pointing os odontoideum compromising the spinal canal. T2 W hyperintense/T1 W isointense lesions noted in upper cervical cord at C2 level measuring about 8 mm in length—suggestive of cord edema/contusion.

Os odontoideum: A well-corticated round area of ossification measuring 7 × 7.5 mm articulating with the anterior arch of atlas. Os odontoideum is seen subluxated to right side in relation to body of the C2 with left lateral angulation at C1–C2 level. No canal compromise. Clivus is short. Evidence of mild basilar invagination without canal compromise. Tip of the dens is just below the McRae line, 5 mm above the Chamberlain and 8 mm above the McGregor line.

Evidence of mild **basilar invagination** with tip of the dens minimally indenting the cervico medullary junction without intra-axial edema. Tip of the dens is 2 mm below the McRae line, 4 mm above the Chamberlain and 8 mm above the McGregor line.

***Persistent hypoplastic vitreous*:** Small right eyeball with retrolental soft tissue lesion and hypoplastic vitreous. Hyaloid remnant of cloquets canal visualised. No evidence of calcifications—features favour persistent hypoplastic primary vitreous. Evidence of vitreous hemorrhage with thin subchoroidal collection.

Spine

Scoliosis: Dorsolumbar scoliosis with convexity to the left. Apical vertebrae is L1. Upper end vertebra is D8. Lower end vertebra is L3. Cobb's angle measures 22°. No structural abnormality in the vertebrae**.**

Sacral agenesis: High bulbous ending cord at upper border of D12 vertebrae level (distal spinal cord hypoplasia). Sacral agenesis involving the lower sacral vertebrae–group I caudal regression syndrome.

Sacroiliitis: Bilateral symmetric sacroiliitis with subchondral erosions, marrow oedema and sclerosis. No evidence of ankylosis—features favour seronegative spondyloarthropathy. Suggested clinical/lab parameter correlation.

Sacroiliitis with ankylosis: Bilateral symmetric sacroiliitis with subchondral erosions, marrow oedema and sclerosis, partial ankylosis in the both sacroiliac joint—features favour seronegative spondyloarthropathy—possible ankylosing spondylitis. Suggested clinical/lab parameter correlation.

Osteitis condensans ilii: Sclerosis of iliac side of bilateral sacroiliac joint without edema/erosion–osteitis condensans ilii.

Dorsal dermal sinus with cutaneous opening in the S1–S2 region coursing anteroinferiorly and extends into the spinal canal at upper part of S1 vertebrae level. Intradural sinus ascends superiorly within the spinal canal through an heterogeneous peripherally enhancing ill-defined intraspinal canal lesion from S1 to L2 levels and attached posterior to the conus at L2 vertebrae level. The intraspinal lesion measures 45 (CC) × 4 (TR) × 6.4 (AP) mm. There is areas of well-defined lobulated cyst (12 × 6 mm) at L5 vertebrae level within the lesion and shows areas of diffusion restriction—suggestive of epidermoid. The lesion does not show peripheral enhancement and leptomeningeal enhancement. 24 × 3 mm size peripherally enhancing infected subcutaneous dorsal dermal sinus at L5, S1 level. Conus ends at L2 vertebrae level.

Myelomeningocele: Evidence of large lumbosacral myelomeningocele with herniation of meninges and

the neural elements through the wide posterior osseous spinal defect at L3 to lower sacrum. Myelomeningocele sac measures 9.5 × 9 cm. Neural elements are seen dangling from the myelomeningocele sac. Mild prominence of the central canal of the cord. There is tethering of the cord. No filum terminale lipoma. No sacral hypoplasia. No vertebral segmentation anomalies. No evidence of cerebellar tonsillar herniation.

Meningocele/terminal myelocystocele: Evidence of large lumbosacral meningocele with herniation of meninges through the wide posterior osseous spinal defect at L3 to lower sacrum. Meningocele sac measures 9.5 × 9 cm. Mild prominence of the central canal of the cord. There is tethering of the cord. No filum terminale lipoma. No sacral hypoplasia. No vertebral segmentation anomalies. Terminal end of cord noted at L3 vertebral level. The sac is covered with skin. Cord ends above the L3 vertebra.

Ventral cord herniation: Anterior herniation of the cord at D5 vertebral level with prominent subarachnoid space in the posterior aspect—suggestive of idiopathic ventral cord herniation.

Diastematomyelia: Evidence of diastematomyelia from D9 to upper border of L3 vertebra and tethering of the cord, with conus ending at L3-L4 level. Bony spur seen at D12–L1 vertebrae level measuring 79 mm (AP) × 6.4 mm (width) × 7.8 mm (CC). Two hemicords unit inferiorly at L3 vertebrae level. Focal syringomyelia of the left hemicord at D12 to L2 vertebrae level.

Lipomyelocele: 41 mm (CC) × 20 mm (TRANS) × 13 mm (AP) size transitional lipoma in the dorsal aspect of the conus extending from L1 to S1 vertebrae level with tethering of cord. Conus ends at lower border of L5 vertebrae level. Transitional lipoma continuous up to the subcutaneous fat through the posterior spinal defect at L4, L5 vertebrae level. Focal syringomyelia (16 × 7 mm) at D12, L1 vertebrae level. No evidence of cerebellar tonsilar herniation.

LDM (limited dorsal myeloschisis): Linear fibro neural tract extending from the dorsal aspect of the conus at upper L2 level and connected to the skin through the small posterior spinal defect at L3–L4 level. There is herniation of the CSF through the same posterior spinal defect with CSF sac surrounding the fibro neural tract in the subcutaneous plane. CSF sac measuring about 20 × 10 mm (saccular type).

Mucopolysaccharidosis: J-shaped sella seen. Multiple prominent VR space noted along the corpus callosum and white matter. Acute kyphosis (Gibbus) at the thoracolumbar junction due to wedging of L1 vertebral body. Platyspondyly. Prominent—postdens soft tissue thickening and posterior ligamentous thickening (thickened dural ring at the foramen magnum) causing narrowing of postdens space and cervical cord compression. No evidence of altered signal intensity in the cervical cord.

Spinal dural arteriovenous fistula (Type I spinal AVM): Prominent dilated serpiginous vessels in the posterior spinal canal of thoracic region, more prominent in the lower dorsal region from D8 to D12 and in the anterior spinal canal from D5 to D11 level. MR angiography shows feeding vessel from D9 to D10 left radicular artery. Cord hyperintensity noted from D8 vertebral level to conus with mild expansion of cord and heterogeneous enhancement—features favour cord edema/ischemia (venous hypertensive congestive myelopathy).

Grade I spondylolisthesis of L5 over S1 with bilateral spondylolysis of L5 pars interarticularis.

Spondylolysis: Defect in the bilateral pars articularis of the L5 vertebra causing grade 1 anterolisthesis of L5 over the S1 vertebra. Sclerosis and degenerative changes noted in the posterior elements of the L5 vertebra. Associated with pseudodisc bulge and mild bilateral neural foramen narrowing.

Hirayama disease: Moderate localized lower cervical cord atrophy at C3 to C6–C7 with cord hyperintensity predominantly involving central, anterior gray matter (C3 on right hemicord and C4 on the left hemicord to C6–C7). Cervical abnormal curvature and symmetric cord flattening noted. Loss of attachment of dorsal dural sac, anterior displacement of the dorsal dura on flexion (from C3 to D1) and a prominent posterior epidural space with a prominent epidural veins which appears as flow void in space sequence. On contrast administration contrast enhancement noted in the posterior epidural component.

Burst fracture noted involving body of D9 vertebra with fracture fragment causing mild narrowing of spinal canal and mild injury to the posterior ligamentous complex (PLC). No evidence of any injury to nerve roots and spinal cord compression—**TLICS-4** (Table 2.10).

Spine trauma: Jefferson fracture: Linear fracture noted on the left and right sides of the anterior and posterior arches of the atlas. Minimal displacement of the posterior arch noted. Atlantodental interval is increased measuring 6 mm.

Locked facet: Dislocation of the left facet joint of C6 behind C7 noted resulting in a unilateral locked facet causing grade 2 anterolisthesis of C6 on C7. Associated rotatory subluxation without dislocation of the right facet joint. No associated fracture is seen on the right side.

Table 2.10: Thoracolumbar injury classification and severity score (TLICS) calculation

Injury morphology	*Point value*	*PLC status*	*Point value*	*Neurological status*	*Point value*
Compression	1	Intact	0	Intact	0
Burst	2	Injury suspected or intermediate	2	Nerve root involvement	2
Translation or rotation	3	Injured	3	Spinal cord or conus medullaris injury Incomplete Complete	 2 2
Distraction	4			Cauda equina syndrome	3

Alignment and articulation of the rest of the cervical vertebra appears normal.

Spinal TB: Altered T2 signal intensity noted involving the body of D6 to D8 vertebrae with collapse and anterior wedging of the D7 vertebra. Loss of intervertebral disc height noted. There is a prevertebral, paravertebral and epidural collection extending from the D5 to L3 vertebral levels. Epidural collection causes narrowing of the spinal canal with compression of the spinal cord at the D6 level. Anterior subligamentous spread noted. Left psoas appears enlarged with a T2 hyperintense collection noted from L2 to L4 levels. On contrast, the collection shows thick, peripheral enhancement. Visualized lung fields show multiple miliary nodules.

Infective spondylodiscitis: D5–D6 disc signal alteration adjacent vertebral marrow signal changes with epidural soft tissue collection causing mild cord compression without significant cord signal abnormality. Lytic destruction of D11 and D12 vertebral bodies with partial collapse of D12. There is involvement of the D11–D12 disc space. Anterior epidural soft tissue thickening at D11–D12 level indenting the cord and extending to the right D11–D12 neural foramina. There is adjacent pre and paravertebral abscess and large right psoas abscess (7 × 6.6 × 20 cm). Right kidney is pushed laterally by the psoas abscess.There is involvement of the adjacent D10 and L1 vertebral bodies. There is marrow edema of pedicles of D11 and D12. Mild scoliosis of lower dorsal spine with convexity to left.

Transverse myelitis: Long segment T2 hyperintensity noted in the cord extending from the C5 to D2 levels. Predominantly central cord involvement noted in the T2 axial images. Cord appears mildly expanded with associated oedema. The rest of the cord appears normal. There is no enhancement on contrast. There is no associated syrinx.

Disc bulge: Disc dessication with diffuse disc bulge noted at the L4–L5 level causing spinal canal narrowing with compression of the ventral thecal sac without causing any significant compression of the nerve roots.

Disc protrusion: Disc dessication with focal right paracentral disc protrusion noted at the L4–L5 level along with facetal arthrosis causing spinal canal narrowing and compression of the right exiting L5 nerve root. No evidence of synovial cyst.

Intramedullary ependymoma: Evidence of intramedullary heterogeneously enhancing mass lesion with cystic areas and hemosiderin rim measuring about 10 × 14 × 62 mm (AP × TR × CC) at lower C2 to upper C7 level. Expanding the cord with cord edema extending up to the lower medulla superiorly and D3 level inferiorly.

Chest

COVID-19: Multiple focal patchy ground-glass opacities with interstitial thickening in bilateral lung fields predominately lower lobe and peripheral involvement—likely viral pneumonitis (CT chest severity score: 10/25), lung involvement 40% (moderate).

Percentage of lobe involved:

1. <5% involvement,
2. 5–25% involvement,
3. 26 to 50% involvement,
4. 51 to 75% involvement,
5. 76 to 100% involvement.

CT severity score: Severe: 16–25, moderate: 9–15, mild: 0–8.

Interstitial pneumonitis: Extensive intralobular and interlobular septal thickening, ground glass opacities in both lungs and minimal traction bronchiolectasis noted in the subpleural interstitium more severe in the basal segments of both lower lobes. Features favour interstitial pneumonitis.

***Usual interstitial pneumonia pattern*:** Subpleural interstitial thickening with early honey combing in both lungs with predominant involvement of the bases.

Crazy paving pattern of ground glass opacities with interstitial thickening in bilateral lower lobe lung with mosaic attenuation in bilateral upper lobe lung with sparing of basal segment—possible **hypersensitive pneumonitis.**

Fibrotic lung disease checklist: Zonal distribution, honeycombing, traction bronchiectasis, reticulations, ground glass opacities, air trapping, cyst, consolidation, emphysema, lymph node, oesophageal dilatation, pulmonary artery size, aorta size, coronary calcification, cardiac chambers, pericardium (thickening/effusion), pleura.

***Neuroendocrine cell hyperplasia (children)*:** There is extensive ground glass opacities with areas of nodules in the central part of bilateral lung with peripheral air trapping—features favour neuroendocrine cell hyperplasia of infancy.

Lobar consolidation: Consolidation with air bronchogram noted in the right upper lobe. Right minimal pleural effusion. No significant mediastinal lymph nodes

***Metastasis*:** Multiple well-defined circumscribed soft tissue dense lesion of varying size with basal predominance noted in the bilateral lung fields. Largest lesion measuring 5 × 6 cm right upper lobe posterior segment and smallest measuring 2 × 1 cm in the superior segment of left lower lobe.

Septic emboli: Multiple well-defined cavitating soft tissue dense nodules with peripheral and basal predominance noted in the bilateral lung fields.

Multifocal pneumonitis: Subsegmental atelectasis with consolidation involving the right middle lobe medial, both lower lobes apical, posterior basal segment with air bronchogram and patchy air space opacities.

***Tuberculosis*:** Centrilobular nodules in tree in bud pattern noted in the apical and anterior segment of right upper lobe. Cavitation with surrounding consolidation measuring 3 × 4 cm noted in the left upper lobe. Right minimal pleural effusion noted. A few enlarged necrotic lymph nodes noted in the right paratracheal region and bilateral hilar region.

Achalasia cardia–post-POEM status: Post-surgical clips noted in the right lateral wall of lower thoracic oesophagus and GE junction. No oral contrast extravasation. No evidence of mediastinal collection/hematoma. Mild dilatation of esophagus. Minimal air seen in the mediastinum and peritoneal cavity. Bilateral minimal pleural effusion with plate atelectasis changes in both bases.

***Lung mass*:** An ill-defined heterogeneously enhancing mass lesion approximately measuring 4.5 × 4 cm noted in the right upper lobe anterior segment with collapse of upper lobe lung parenchyma. Abrupt cut-off of right upper lobe bronchus. No satellite lesion/interstitial thickening/pleural effusion/mediastinal lymphadenoapthy noted, the lesion shows no contact with mediastinum and pleura. Chest wall appears normal.Visualized skeleton appears normal. A few enlarged lymph nodes noted in the right paratracheal region. Visualised supraclavicular region, liver and adrenals appear normal (staging T3N0M0).

Checklist: Location, appearance (solid, part solid, ground glass), size, infiltration of adjacent structures (aorta, pericardium, heart, bronchus, carina, diaphragm, pleura, mediastinal fat), lymph nodes, intra and extra thoracic metastases.

Mediastinal lymphoma: Evidence of soft tissue density lesion in the right lower neck and superior mediastinum measuring about 4.9 × 4 × 9 cm encasing the right common carotid artery, IJV, subclavian and brachiocephalic artery and vein, vertebral artery, superior vena cava , ascending aorta and arch of aorta. Trachea is mildly pushed to left side without significant compromise of the airway.

Scimitar syndrome (pulmonary venolobar syndrome): There is volume loss of right lung with mediastinal shift to the right and dextro position of heart. Right superior pulmonary vein is seen draining abnormally into the azygos vein, SVC and another abnormal right inferior pulmonary vein is seen draining into the IVC giving scimitar-like appearance. There is an abnormal arterial feeding vessel to the right lung parenchyma which is arising from the coeliac trunk. Left superior and inferior pulmonary veins are draining into the left atrium. Main pulmonary and left pulmonary arteries appear normal. Measurements (diameter in mm): Scimitar vein; Proximal–7.0, Distal–7.8. Right pulmonary artery: Proximal–8.9, Distal–8.0. Left single pulmonary venous trunk: Proximal–5.4, Distal–2.6. Left pulmonary artery: Proximal–7.3, Distal–6.2.

Acute pulmonary thromboembolism: Main pulmonary artery and its bifurcation appear normal. There is evidence of multiple embolism in right main pulmonary artery, interlobar right lower lobe segmental arteries, left main, left upper lobes and right lower lobe segmental arteries with irregular surface. Size of thrombus measures from 3 to 16 mm. No evidence of total occlusion. Most of thrombus in right lower lobe segmental artery lies freely within the lumen with contrast medium seen surrounding thrombus. Main, right and left pulmonary artery dimensions are within normal limits. No CT evidence of pulmonary arterial hypertension. No evidence of pulmonary infarction. No evidence of consolidation.

Comment about caliber of pulmonary arteries (main trunk, left main branch, right main branch), right heart strain, pulmonary infarction, patency of airways, pleura, pericardium, upper abdomen.

Cardiovascular System

Major aortopulmonary collateral arteries (MAPCAs): Multiple MAPCAs from left subclavian artery. Proximal MAPCA is large and descends down vertically supplying the left lung. Right subclavian artery proximal segment shows a moderate sized MAPCA looping up and descending down. Large MAPCA supplying the confluence arising from the distal arch of aorta. Moderate sized MAPCA arising from descending thoracic aorta at D7 level. Right pulmonary artery measures 11.4 mm. Left pulmonary artery measures 9.8 mm. Main pulmonary artery measures 9.1 mm. Ascending aorta measures 29 mm.

***Ascending aortic aneurysm*:** Ascending aorta measures 4.1 cm with eccentric thrombus suggestive of fusiform aneurysm for a length of 7.6 cm till the origin of brachiocephalic artery. Patent lumen measures 3.1 cm. Arch measures 3.7 cm. Descending thoracic aorta measures 3.7 cm. Abdominal aorta at hiatus measures 3.9 cm. Infrarenal aorta measures 2.3 cm (Table 2.11).

***Coronary arteriovenous fistula*:** Right coronary artery co-dominant and normal. Right posterior descending artery is normal. Separate origin of large conal branch with ectatic segment and communicating with MPA suggestive of coronary to pulmonary AV fistula. The fistula also communicates with first septal from LAD.

Anomalous coronary artery: Left anterior descending coronary artery: Arises from right coronary trunk courses anterior to aorta and pulmonary artery to enter interventricular groove (Type I course). It gives off two diagonals and septals. Type III vessel with 50–60% ostial stenosis and 20–30% stenosis in mid segment. Diagonals are normal. Left circumflex coronary artery: Nondominant; courses posterior to aorta and pulmonary artery. It is small and normal. Right coronary artery: Dominant with mild midsegment irregularities.RV branch continues as PDA and is normal. Large PLV is normal.

Aortic dissection: Dissecting aneurysm involving the distal arch of aorta, distal to the left subclavian artery with intimal flap extending up to the infrarenal abdominal aorta, 3 cm prior to bifurcation. Aortic bifurcation appears normal: Type B Stanford classification. No evidence of aortic wall irregularity/pleural and pericardial hyperdense haematoma to suggest rupture. No evidence of thrombus. SMA, inferior mesenteric artery, right main and accessory renal artery arising from the false lumen. Dissection intimal flap extending to the proximal left renal artery. No evidence of altered perfusion in the kidneys. Tortuous course of descending thoracic aorta seen.

Coarctation of aorta: Ascending aorta measures 26 mm. Arch measures 19 mm. Coarctation noted at D4 level measuring 8.2 mm proximal to the PDA, PDA measures 8 mm in length with 6.8 mm in diameter. Pre-ductal segment of aorta measures 14.8 mm. Post-ductal aorta measures 14.6 mm. Prominent D4, D5, D6 intercostal vessels noted. MPA measures 36 mm. RPA measures 18 mm. LPA measures 15.4 mm. Origin of innominate artery, left common carotid artery and left subclavian artery appear normal.

Transposition of great arteries: Concordant veno arterial connection. Discordant atrioventricular and ventriculo-arterial connection. Aorta is seen anterior and to the left of main pulmonary artery: Levo transposition of the great arteries (L-TGA). Left and right ventricles with their corresponding anteroventricular valves are also transposed. Atrial septal defect measuring about 10.1 mm. Ascending aorta measures 23 mm. Dilated left atrium and appendage. Mildly dilated IVC (24 mm). Right atrium is small. Morphologic right ventricle seen in the left side with prominent trabeculations. Mild hypokinesia of the apical and apex of the left side of ventricle. Altered signal intensity in the myometrium of the left ventricle predominantly involving the anterior wall. No evidence of delayed enhancement. Pulmonary infundibulum hypertrophy with lumen measuring ~2 cm. Main pulmonary artery measures 33 mm. Left pulmonary artery measures 20 mm. Right pulmonary artery measures 13 mm. Main pulmonary artery partly overrides the left ventricular outflow.

Trans catheter aortic valve implantation workup: Cuspidity of native valves, leaflet calcifications, subvalvular calcifications, Agatston score of leaflet calcification, aortic

Table 2.11: The aortic measurements at various levels—sample reporting format

Level	*Dimensions*	*Level*	*Dimensions*
Aortic sinus	42 mm	Descending thoracic aorta	40 mm
Ascending aorta	38 mm	Suprarenal abdominal aorta	32 mm
Proximal to aortic arch	29 mm	At the level of renal arteries	25 mm
Midaortic arch	29 mm	Infrarenal abdominal aorta	22 mm
Just distal to left subclavian artery	50 mm		

anulus measurements both in systole and diastole, annular short and long axis diameter in mm, annular perimeter in mm, annular area in mm^2, inner diameter of degenerative prosthetic valve in mm (for valve in valve procedure), aortic sinus height, width, distance from annular plane to left and right coronary ostium, diameter of sinotubular junction, maximum cross sectional diameter of ascending aorta, comment about patency and luminal diameter of brachiocephalic, subclavian, common iliac, external iliac and common femoral artery.

Concentric left ventricular hypertrophy: The left ventricular myocardium shows concentric hypertrophy. The observed LV mass is 245 gm and the BSA indexed mass (119 gm/m^2) qualifies for hypertrophy as per echo guidelines (>114 gm/m^2). The LV posterior wall and inter-ventricular septum each measure 16 mm in thickness in diastole. There is no dyskinesia/failure to thicken of any of the LV myocardial segments. And all the LV cardiac segments contract well. The inter-ventricular septum is intact.

Conclusions

1. Significant concentric left ventricular hypertrophy suggesting long standing systemic hypertension.
2. Normal cardiac anatomy and myocardial function.

Noncompaction cardiomyopathy: Mild dilatation of left ventricle. Moderate dilatation of left atrium. Global hypokinesis of the left ventricle. Prominent trabeculation noted in the endomyocardium of apex and mild left ventricular cavity. Basal left ventricle is relatively spared. Mild delayed enhancement of the endocardium. Minimal mitral regurgitations seen.

MRI analysis shows: End diastolic (ED) volume–78.2 (ml/m^2). End systolic volume–54 (ml/m^2). Stroke volume–23.3 (ml/m^2). Cardiac index–1.86 (min/m^2).

Table 2.12: Measurements from SSFP images acquired during diastole

Diameter in mm	*Proximal*	*Distal*
Main pulmonary artery	18 × 20	
Aortic annulus	24 × 28	
Aortic sinus	39 × 40	
Sino-aortic Jn	30 × 32	
Ascending aorta	32 × 33	

Myocardial mass at ED–67.2 (gm/m^2). Myocardial mass average–68.2 + 5.5 (gm/m^2). Ejection fraction–29.8%.

ARVD/C: Some regions of the **anterior wall of the right ventricle is thinned** out. The RVOT is dilated (31 mm × 34 mm), **dyskinetic and shows systolic anterior bulge**. Apart from the RVOT, there is an area in the **sub-tricuspid region which is also dyskinetic.** The BSA indexed RV end diastolic volume is increased to more than the normal, the end-systolic volume to about twice the normal. **There is global index of RV contractility (RVEF = 23–26%).** The right atrium is mild dilated. The interatrial septum is intact. There is mild tricuspid regurgitation (about 6–9 ml/heart beat, difference in the stroke volumes). The venous drainage, atrio-ventricular and the ventriculo-arterial connections are concordant. The atrio-ventricular valves and the semilunar valves function normally without any stenosis or regurgitation. The inter-atrial and the inter-ventricular septae are intact. The aortic arch is left sided and has normal branching pattern. The main pulmonary artery and its branches have normal caliber. The left atrium is not dilated. The left ventricle has upper limits of normal body surface area indexed end diastolic volume. The indexed LV end systolic volume is about 1 and ½ times the upper limits of normal due to global hypokinesia and IVS dyskinesia. The IVS is thinned out. The IVS is also dyskinetic. The

Table 2.13: Ventricular volume measurements (Heart rate: 77 /min)

	EDV (mL)	*ESV (mL)*	*SV (mL/beat)*	*EF%*	*Ventricular CO (L/min)*
LV	80	28	52	65	4.03
RV	80	26	54	68	4.22
Indexed ventricular volume measurements					
Male standards	*EDV (mL/ m^2)*	*Normal EDV*	*ESV (mL/m^2)*	*Normal ESV*	*Ventricular CI (L/min/m^2)*
LV	39	47–92	14	13–30	1.95
RV	39	55–105	13	15–45	2.05
Great vessel flow (Heart rate: 77/min)					
	FF (mL/beat)	*BF (mL/beat)*	*Net FF (mL/beat)*	*RF%*	*Arterial flow (L/min)*
Aorta	63	4	59	7	4.62
MPA	62	2	59	4	4.60

CO–cardiac output, CI–cardiac index

index of systolic function is significantly depressed (LV EF = 26%). Some areas of the septum also show delayed enhancement suggesting myocardial fibrosis. **The features will fit in with a major criteria for ARVD/C from MRI point of view as per 2010 revised guidelines (regional wall movement abnormalities and RV dysfunction).**

Endocardial myofibrosis: Endocavitatory filling defect in the apex of right ventricle obliterating the ventricular apex with no enhancement consistent with thrombus/fibrosed soft tissue. Systolic dysfunction in SSFP and gradient sequences of the right ventricular apex noted. Moderate dilatation of both atrium (Right > Left). Thickened soft tissue in the apex of right ventricle with compromised right ventricular cavity. Thin rim of enhancement along the endocardial aspect of right ventricle in the delayed images.

Situs solitus with levocardia. Mild to moderate mitral and tricuspid regurgitation. Dilated IVC and hepatic vein. Global hypokinesia of the left ventricle. No evidence of perfusion defect. RV and LV appear smaller in size. RV apex and LV apex obliterated due to focal thickening.

Ejection fraction of LV is 29%. 16 × 8 mm size non enhancing hypointense lesion ventricular cavity at the anterior wall of left ventricle near the apex with perfusion defect—thrombus. Delayed contrast enhancement study shows mild endocardial enhancement along the basal and mid-LV cavity and intense enhancement along the endocardium in the apical and apex of RV and LV. Patchy transmural enhancement of the apical, anterior and anterolateral wall of left ventricle.

Infarct/scar in the basal inferolateral, basal anterolateral, mid anterior, mid inferoseptal, mid inferolateral, mid anterolateral, apical septal, apical lateral segments of left ventricle with more than 50% of thickness involvement—non-viable myocardium. Rest of the LV is to be assessed for reversible perfusion defects in stress perfusion if indicated (Table 2.14).

Hypokinesia/akinesia with perfusion defect and delayed contrast enhancement involving subendocardial region (>50%) of basal inferoseptal, basal inferior, basal inferolateral, mid anterior, anteroseptal, inferior, apical anterior, septal, lateral and apex suggestive of infarct (nonviable myocardium). Aneurysmal dilatation of left ventricular apex. Situs solitus with levocardia.

Mammogram

Breast mass: **X-ray mammogram:** Ill-defined radiodense lesions with spiculated margins and internal micro calcifications noted in UOQ of right breast at 11 o' clock position zone II 4 cm depth from skin . Diffuse dermal thickening noted. Nipple and subareolar tissues are normal on the left side.The pectroralis and retro mammary space appears normal. Rounded dense right axillary lymph nodes are seen. **Ultrasound screening:** Irregular hypoechoic mass lesion with internal micro calcifications measuring 4.1 × 3.8 × 2.8 cm noted predominantly in UOQ of right breast. There is extension of the lesion to subcutaneous tissue. With Doppler there is internal vascularity. The left breast shows normal fibrogandular tissues. Enlarged rounded lymph nodes with thickened cortex largest measuring 22 × 15 mm noted in right axilla-**BIRADS V.**

Fibroadenoma: Well-defined hypoechoic lesion measuring about 33 × 20 mm in size seen in the UOQ of the right breast at 10–11 o'clock position. Minimal intralesional vascularity noted. **This lesion is characterized as probable benign (BIRADS category –III)-Fibroadenoma to be considered.**

Gynecomastia: **X-ray mammogram:** Asymmetric increased glandular tissue noted in right breast. **Ultrasound screening:** Retroareolar diffuse hypoechoic tissue noted in both breast (R > L)—findings consistent with glandular tissue. No focal lesions noted. No abnormal vascularity seen.

Breast imaging reporting and data system (BIRADS): Grade 1–Negative. Grade 2–Benign. Grade 3–Probably benign. Grade 4–Suspicious abnormality. Grade 5–Highly suggestive of malignancy. Grade 6–Known biopsy proven malignancy.

Abdomen

Acute edematous pancreatitis: Pancreas appears bulky with peripancreatic inflammation extending to the gastro colic ligament, lesser omentum and left Gerota's fascia. No evidence of pancreatic necrosis/pseudocyst/pancreatic calcification/pancreatic duct dilatation/CBD, GB, pancreatic duct calculus/pseudoaneurysm in adjacent vessels/thrombosis of splenic and portal vein/pancreatic divisum. No biliary dilatation/radiodense CBD calculus.

Mild ascites. Bilateral mild pleural effusion (left >right) with underlying lung parenchymal changes. Above features favour acute edematous pancreatitis. Modified CT severity index 2/10.

Modified CT severity index: Scores are generated by estimating pancreatic inflammation and necrosis to give a score out of 10.

Pancreatic inflammation: 0–normal pancreas, 2–intrinsic pancreatic abnormalities with or without

Table 2.14: Structural and morphology left ventricle on cardiac MRI

Lateral ventricle segments	*Trabeculation*	*End diastolic (mm)*	*Endsystolic (m)*	*Wall motion*	*Dynamic perfusion*	*Delayed hyper-enhancement*	*Stress perfu-sion*	*Impression*
Basal anterior	P	6.9	11.3	Normal	Normal	No	Not done	Normal/RPD
Basal anteroseptal	A	10.4	13.8	Hypokinesia	MPD	<25 % thickness		Infarct/scar
Basal inferoseptal	A	8.2	8.2	Akinesia	MPD	Transmural		Infarct/scar
Basal inferior	A	5.9	5.8	Akinesia	MPD	Transmural		Infarct/scar
Basal inferolateral	A	3.4	4	Akinesia	MPD	Transmural		Infarct/scar
Basal anterolateral	P	6.3	7.5	Normal	Normal	No		Normal/ reversible perfusion defect
Mid anterior	P	7.9	9.2	Normal	Normal	No		Normal/ reversible perfusion defect
Mid anteroseptal	T	6.9	9.2	Hypokinesia	Mild	25–50%		Infarct/scar
Mid inferoseptal	A	5.7	5.2	Akinesia	PD	Transmural		Infarct/scar
Mid inferior	A	2	2.2	Akinesia	PD	Transmural		Infarct/scar
Mid inferolateral	A	2.2	2.1	Akinesia	PD	Transmural		Infarct/scar
Mid anterolateral	P	6.8	15	Normal	Normal	Normal		Normal/RPD
Apical anterior	P	6.7	13	Normal	Normal	Subendocardial		Infarct/scar
Apical septal	A	4.8	10	Hypokinesia	MPD	50% thickness		Infarct/scar
Apical inferior	A	3.1	3.2	Akinesia	PD	Transmural		Infarct/scar
Apical lateral	P	7.8	10.3	Hypokinesia	MPD	Transmural		Infarct/scar
Apex	T	2.3	4.3	Hypokinesia	--------	Transmural		Infarct/scar

A–absent, P–present, MPD–mild to moderate perfusion defect, RPD–reversible perfusion defect; PD–perfusion defect

*Normal/reversible perfusion defects are assessed with stress perfusion.

*Segmental wall thickness = ES–ED/ED × 100

*Patterns of delayed enhancement–subendocardial/transmural/patchy/linear midwall/epicardial zone. 1 to 25% thickness enhancement (subendocardial). 25 to 50% thickness enhancement. 50 to 70% thickness enhancement. More than 70% thickness enhancement (transmural).

inflammatory changes in peripancreatic fat, 4–pancreatic or peripancreatic fluid collection or peripancreatic fat necrosis.

Pancreatic necrosis: 0–none, 2–30% or less, 4–more than 30%.

Extrapancreatic complications: 2–one or more of pleural effusion, ascites, vascular complications, parenchymal complications and/or gastrointestinal involvement.

Total score: Total points are given out of 10 to determine the grade of pancreatitis and aid treatment. 0–2: mild, 4–6: moderate, 8–10: severe.

USG–acute pancreatitis: Altered echoes in the pancreas with peripancreatic inflammation and left Gerota's fascia thickening. No evidence of pancreatic calcification/calculi/pancreatic duct dilatation—features favours acute pancreatitis.

Chronic calcific pancreatitis: The parenchyma of the neck, body and tail of the pancreas is completely atrophied with dilated and tortuous pancreatic duct. Main pancreatic duct and its branches are dilated with maximum diameter of……mm. Multiple irregular calculi noted within the dilated main pancreatic duct and side branches. Calculus in the neck of pancreas measures ....mm. No parenchymal calcification noted. The pancreatic parenchyma of head and uncinate process are preserved. No altered signals noted within the head and uncinate process. The peripancreatic fat is preserved. The peripancreatic vascular system appears normal. No perivascular cuff noted. No peripancreatic collections.

No stricture of CBD/ IHBRD. No vascular complications like venous thrombosis, pseudoaneurysm formation or splenic infarcts.

***Pancreatic divisum variant*:** Persistent communication between the ventral and dorsal pancreatic ducts.

Pancreatic divisum with mild dilatation of dorsal moiety duct maximum measuring mm. Ventral moiety duct narrowing with focal ductal dilatation measuring mm. Presence/absence of intraductal calculus with/ without intrapancreatic and peripancreatic fluid collection measuring about cm and inflammation extending into the portion of duodenum.

***Carcinoma pancreas*:** Ill-defined heterogeneously enhancing mass lesion approximately measuring 2.4 × 2.3 × 3 cm (AP × TR × CC) noted in the head of the pancreas. The lesion causes abutment of superior mesenteric, splenic, portal vein confluence. No evidence of regional lymph node enlargement, peritoneal deposit, liver lesions, ascites. Celiac artery, superior mesenteric artery, portal vein shows normal opacification. No evidence of distant metastatic nodules in the spleen, adrenals, visualized lung fields, vertebra and pelvic bones.

Carcinoma pancreas–reporting checklist: Morphology: Appearance (in pancreatic parenchymal phase): Hypo/ iso/hyper attenuating; Size: Maximal diameters in axial and transverse; Location: Head, uncinated, body or tail; Pancreatic duct status: Presence of abrupt narrowing/ cut off. Presence or absence of upstream dilatation, ductal calculus if any with maximum diameter of the duct. Biliary tree: Cut off/ dilatation, perineural spread. **Arterial evaluation (SMA, celiac axis, common hepatic artery, variant vessel):** Vessel degree of solid soft tissue contact (<180 or >180 degrees), degree of haziness/stranding contact (<180 or >180 degrees), focal narrowing/contour irregularity (+/–), extension to branches/bifurcation (+/–). **Venous evaluation:** Vessel degree of solid soft tissue contact (<180 or >180 degrees), Degree of haziness/stranding contact (<180 or >180 degrees), Focal narrowing/contour irregularity (+/–), extension to branches/bifurcation (+/–), extension to first draining vein, thrombus within vein. **Extra pancreatic evaluation:** Liver lesions, peritoneal/omental lesions, ascites, suspicious lymph nodes, extra pancreatic adjacent structure involvement.

***Serous cystadenoma pancreas*….**mm size measuring multilobular cystic lesion with central scar and calcification in the head and uncinate process of pancreas. The lesion causes mass effect on MPD resulting in dilatation (mm in the body of pancreas) of main pancreatic duct.

Mucinous cystadenoma: Evidence of well-defined exophytic cystic lesion measuring about 5.5 × 3.9 × 3.5 cm in the anterior aspect of the head/neck of the pancreas. Thin septa with calcification seen within. No evidence of solid areas/surrounding inflammation. Lesion is communicating with the main pancreatic duct (a rare feature in mucinous cystadenoma). (Even though cyst is communicating with the MPD, possibility of IPMN is less likely due to the presence of calcification.)

Insulinoma: A well-defined strongly enhancing lesion measuring 4 × 6 mm noted in the body of pancreas. No calcification noted within the lesion. Strongly enhancing small lesion in pancreas—to rule out insulionoma.

Extra pancreatic evaluation: Liver lesions, peritoneal/ omental lesions, ascites, suspicious lymph nodes, extra pancreatic adjacent structure involvement.

Cirrhosis liver: Liver is shrunken in size measures 8.5 cm with atrophy of the anterior segment of the right lobe and hypertrophy of the caudate lobe and lateral segment of left lobe. The caudate lobe to right lobe ratio is 0.87 (more than 0.65 definite sign of cirrhosis). There is widening of the fissures for ligamentum teres and ligamentum venosum. There is evidence of posterior hepatic notch noted in segment VI. Diffuse heterodense liver parenchyma with surface nodularity. No evidence of intra or extra hepatic biliary radicle dilatation. No arterial phase enhancing mass lesion to suggest hepatocellular carcinoma. Partial thrombosis of the main portal vein extending into the right and left intrahepatic branches. Main portal vein is enlarged and measures in mm. The superior mesenteric vein appears dilated, measures in mm. The splenic vein appears dilated measures in mm. Portosystemic collaterals noted in splenic hilum, lieno-renal ligament and around the GE junction. Left renal vein is normal. Features are suggestive of cirrhosis liver with portal hypertension and portosystemic collaterals. No arterial phase enhancing mass lesion to suggest hepatocellular carcinoma.

Portal hypertension (Doppler): Liver appears shrunken with coarse echoes, irregular surface blunted margins, portal vein measures 12 mm at hilum, no evidence of filling defect in the main portal vein. Portal vein velocity 12 cm/s hepatopetal flow, multiple dilated tortuous splenohilar and splenorenal collaterals. Hepatic veins patent shows monophasic flow. Free fluid noted in the pelvis.

Hepatocellular carcinoma: A round T2 hyperintense lesion, showing restricted diffusion measuring 21 × 40 mm noted in segment VI of liver. The lesion shows significant nonrim arterial phase enhancement with

washout in portal venous phase, it shows capsular enhancement in equilibrium phase, the size of the lesion has doubled compared to previous imaging taken 6 months back-**LI-RADS: LR-5 (definite HCC).**

Checklist for HCC: Location (mention the segment), size, tumoral thrombus, nonrim arterial phase hyper enhancement, threshold growth, nonperipheral washout appearance, enhancing capsule appearance, lymph node status, remaining abdomen for extrahepatic mass.

Cholelithiasis: Multiple small GB calculi without diffuse gall bladder wall thickening. No evidence of CBD calculus/CBD, IHBR dilatation/pancreatitis/pericholecystic fluid collection. Features favour cholelithiasis.

Calculus cholecystitis: Multiple small GB calculi with diffuse gall bladder wall thickening (4.2 mm). No evidence of CBD calculus/CBD, IHBR dilatation/pancreatitis/pericholecystic fluid collection. Features favour acute calculus cholecystitis.

Klatskin's tumor: Soft tissue lesion in the confluence of hepatic ducts and proximal CHD causing dilatation of right hepatic duct (… mm in diameter), left hepatic duct (…. mm in diameter) and IHBR. No evidence of periportal/paraaortic lymphadenopathy/focal liver mass lesion. The mass lesion encasing the left hepatic artery and left branch of portal vein causing moderate to severe luminal narrowing. Total length of RHD, LHD and CHD involvement is ....mm. Features favour Klatskin's tumor (Type IV).

Mass forming intrahepatic cholangiocarcinoma: Evidence of well-defined irregular infiltrating heterointense mass lesion measuring about 7.2 × 5.7 × 7.8 cm in segment VIII of right lobe of liver. Lesion is mildly extending to segment IVA and VII of liver. It is indenting right hepatic vein and middle hepatic vein without infiltration. It is Infiltrating and narrowing hepatic duct confluence, RHD and its divisions, proximal LHD and CHD with bilobar intrahepatic biliary dilatation. CBD is not dilated. Tumor is extending to right branch of portal vein. Main portal vein and left branch are normal. It is encasing the right branch of hepatic artery. On contrast administration, mass shows thick irregular peripheral rim enhancement in arterioportal phase with peripheral wash out, central enhancement in delayed images and hepatobiliary phase. Features are consistent with mass forming intrahepatic cholangiocarcinoma (MF-ICC) in right lobe of liver with biliary and portal vein invasion.

Cholangiocarcinoma checklist: Size (maximal axial dimensions in cm), location (upper/mid/lower third of bile duct), hepatic duct involvement (right/left/both). Second-order ductal branch involved and side: (yes/no; right/left), arterial evaluation: Common/hepatic artery proper involvement, portal vein involvement, solid soft tissue contacts, focal vessel narrowing or contour irregularity, aberrant/accessory arterial anatomy: (yes/no—specify), venous variants. Lymph nodal enlargement (>1 cm short axis), bile duct variants, remnant liver volume and distant metastases.

Mirizzi syndrome: ….mm calculus in the cystic duct –CBD junction causing dilatation of CHD (…mm in diameter). Right hepatic duct (…mm in diameter) left hepatic duct (…mm in diameter) and IHBR—possible Mirizzi syndrome.

Type I choledochal cyst: Disproportionate diffusely dilated CHD, CBD, and distal hepatic ducts with multiple hypointense filling defects in the mid and distal CBD suggestive of calculi (largest measuring 7 mm). Mild dilatation of cystic duct and IHBR—features suggestive of Type 1 Choledochal cyst.

Type IVA choledochal cyst: Moderate dilatation of CBD, CHD, proximal right and left hepatic ducts (left > right) with abrupt change to normal calibre of the biliary radicles. Another focal cystic dilatation of segment II intrahepatic bile duct: Type IVA choledochal cyst.

Protein losing enteropathy: Mild dilatation of long segment midsmall bowel loops (jejunoileal region, predominantly involving jejunum) in the left lumbar and left iliac fossa with mild increased vascularity. It shows increased contrast enhancement and thickening of the bowel wall, with the clinical presentation of hypoproteinemia and above radiological features, the following protein losing enteropathy to be considered. Intestinal lymphangiectasia/malabsorption syndromes like celiac disease, tropical sprue/eosinophilic gastroenteritis/food-induced enteropathy. Imaging, however, cannot differentiate these conditions.

Ileocecal TB: Diffuse thickening of terminal ileum (9.1 cm length, 1.4 cm thickness), ileocecal junction, caecum (5.4 cm in length) with pericaecal mesentery fat stranding and multiple pericolic lymph nodes predominantly in the ileocolic mesentery. Diffuse narrowing of the lumen. No focal collection in the adjacent mesentry. Ileocecal junction appears pulled up. Appendix is distended with fluid. Few enlarged lymph nodes seen in the ileocolic mesentery. **Possibilities include:** 1. Tuberculosis, 2. Inflammatory bowel disease.

Active inflammatory bowel disease: Diffuse thickening of terminal ileum (9.1 cm length, 1.4 cm thickness), ileocecal junction, caecum (5.4 cm in length), proximal jejunum, transverse colon and midileum with pericaecal

mesentery fat stranding and multiple pericolic lymph nodes predominantly in the ileocolic mesentery. Ileocecal junction appears normal in position. Appendix is distended with fluid and shows heterogeneous enhancement. On contrast administration shows prominent mucosa and submucosa enhancement with prominent vasa recta. No obvious evidence of stricture/sinus tract/fistulous tract/submucosal fat halo seen. No obvious evidence of perianal fistula/sacroilitis—features favour active inflammatory bowel disease—possible Crohn's disease.

Mesenteric panniculitis: A marginally defined subtle increased fat density lesion noted involving the root of the small bowel mesentery encasing the superior mesenteric vessel and its branches. No narrowing or infiltration of the vessels noted. No fibrosing component noted. The above features are suggestive of mesenteric panniculitis.

Umbilical sinus: Umbilical sinus seen measuring …. No significant abscess formation. No obvious evidence of intraperitoneal extension. No evidence of persistent uracus/vitellointestinal duct. **Omphalitis:** Focal thickening of the umbilicus measuring 12 × 10 mm. No evidence of intraperitoneal extension. No evidence of urachal remnant seen—features favour infection (omphalitis). **Urachal remnant:** Tubular channel extending from the dome of bladder along the anterior abdominal wall in the midline toward the umbilicus, representing a urachal remnant.

Incisional hernia: Left para-umbilical incisional hernia with omentum and bowel as content. No evidence of bowel obstruction/strangulation. **M3W2**.

Hirschsprung disease: Reversal of recto sigmoid ratio with more dilatation of sigmoid compared to rectum. No transitional zone identified—possibility of Hirschsprung disease to be considered.

Table 2.15: Incisional hernia reporting format

Midline	Subxiphoid	M1	
	Epigastric	M2	
	Umbilical	M3	
	Infraumbilical	M4	
	Suprapubic	M5	
Lateral	Subcostal	L1	
	Flank	L2	
	Iliac	L3	
	Lumbar	L4	
Recurrent incisional hernia—YES or NO			
Length: ……cm		Width :……..cm	
Width (cm)	W1 (<4 cm), W2 (≥4–10 cm), W3 (≥10 cm)		

Appendicitis (USG): Probe tenderness noted in the right iliac fossa. Tubular, blind ending, nonperistaltic bowel loop with maximum diameter of …..mm with significant surrounding inflammation noted in the right iliac fossa suggestive of inflamed appendix.

Acute appendicitis (CT): Thickened oedematous appendix (….cm thickness) with minimal periappendiceal inflammation—features favour retrocecal acute appendicitis. No evidence of periappendicular abscess/mass lesion/appendicolith.

Carcinoma stomach: Abnormal wall thickening with luminal narrowing in distal body and antropyloric canal of stomach with maximum thickness measures 3.8 cm. There is gastric outlet obstruction with retained food particles in the overdistended stomach. No periserosal infiltration. No infiltration of the pancreas/liver. A few adjacent perigastric lymph nodes seen, largest measuring about 12 × 10 mm. No significant enlarged celiac, para aortic lymph nodes. A few tiny oval-shaped lymph nodes in the portocaval and paracaval regions. Diffuse omental fat stranding noted. (**Stage T2N1 Mx)**.

CA rectum growth: Circumferential wall thickening (10 mm in thickness) in rectum for a length of 28 mm, about 6.5 cm from the anal verge. The lesion involves predominantly in the anterior rectal wall from 3 o' clock to 9 o' clock position. Lower end of the lesion is 2 mm from the horizontal portion of levator ani and 13 mm from the funnelled portion of levator ani. 7 × 5 mm size solitary enlarged lymph node in the right mesorectal fat at 8 o'clock position. Puborectalis muscle appears normal without infiltration. Internal and external anal sphincters appear normal. No infiltration of the seminal vesicles/prostate/bladder. Mesorectal fascia/Denonvilliers fascia/Waldeyer's fascia appear intact. **(colonic rads–C4/staging work up T3aN1) M staging cannot be ascertained due to limited study).**

Carcinoma rectum check list: Morphology (solid polypoid/solid annular/mucinous), in case of circumferential tumor mention the involvement in clock position. The distance of lesion from the anal verge and anorectal junction, location of lesion with respect to anterior peritoneal reflection (tumors located above the anterior peritoneal reflection in the peritonealised anterior wall do not need surgical resection unless it has invaded adjacent structures), circumferential resection margin, extramural venous invasion (>3 mm), longitudinal, cranio-caudal and largest lesion diameters, perirectal fat invasion and spiculation. Involvement of anal sphincters, presacral fascia and mesorectal fascia (a distance of the tumor to the mesorectal fascia of <1 mm is regarded unsuitable

for total mesorectal excision). Extramural invasion depth (based on the depth of invasion <1 mm, 1 to 5 mm, 5 to 15 mm and >15 mm T3 stage divided into T3a, b, c and d respectively) determines the need for neoadjuvant radiation >5 mm consistent with poor prognosis, nodal spread. **Post-neoadjuvant treatment**: Look for residual tumor mass in the T2W-MR images and give **yTNM** staging.

Carcinoma of anal canal: Eccentric wall thickening (14 mm in thickness) in the anal canal for a length of 31 mm, about 31 mm from the anal verge. The lesion predominantly from 11 o'clock to 7 o'clock position. Lower end of the lesion is well below the horizontal portion of levator ani. Involvement of intersphincteric plane/mass is infiltrating the left obturator internus muscle. Presence/absence of post-operative changes with fibrosis seen in the presacral region/rectal bed**.**

***Pilonidal sinus*:** Evidence of a subcutaneous fluid filled sinus tract noted in the midline in the intergluteal cleft (at the level of lower sacrum at S3–S4) extending inferiorly for about 4 cm and end blindly posterior to the sacrococcygeal junction. No evidence of fistulas communication with the spinal canal. No evidence of enteric (anus and rectum) communication or extension to the ischiorectal or ischioanal fossa. No evidence of secondary tract.

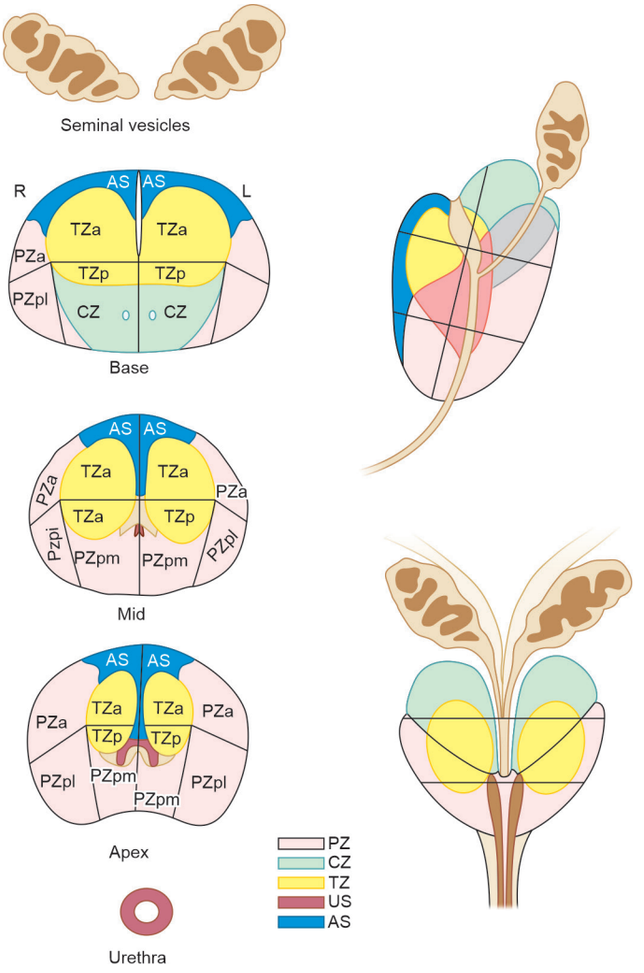

Fig. 2 8: Prostate anatomical zones for reporting

***Perianal fistula*:** Fluid-filled left low perianal intersphincteric fistula with external opening 3 cm from the anal verge and internal opening at 12 o' clock position 1 cm from the anal verge. Total length of the fistulous tract is 38 mm. No evidence of horseshoe tract/secondary tracts/translevator and supralevator extension/ischiorectal and ischioanal abscess—**Grade I** low left perianal fistula (St. James Hospital MR classification).

Fluid-filled left low perianal trans-sphincteric fistula with external opening 12 mm from the anal verge and internal opening at 5 to 6 o' clock position 24 mm from the anal verge. Total length of the fistulous tract is 34 mm. No evidence of horseshoe tract/secondary tracts/translevator and supralevator extension/ischiorectal and ischioanal abscess—**Grade III** low left perianal fistula (St. James Hospital MR classification).

Complex fluid-filled right low perianal trans-sphincteric fistula with external opening 25 mm from the anal verge in the right posterior perineum at 7 o'clock position. The tract extends anterosuperiorly and pierce the external sphincter at 6 to 7 o'clock position and internal opening 6 o'clock position and 24 mm from the anal verge. There is another right lower intersphincteric tract coursing at 6 o'clock position joints with the upper trans-sphincteric tract in the intersphincteric plain at 6 o'clock position 24 mm from the anal verge. Then the common tract extending to the bilateral intersphincteric plain. Right intersphincteric plain tract pierces the external sphincter at 10 o'clock position no significant collection in the right ischioanal abscess. Left intersphincteric tract ends at 3 o'clock position. No evidence of translevator and supralevator extension/ischiorectal and **Grade IV** low right perianal fistula (St. James Hospital MR classification).

***Checklist*:** Number of fistula openings, internal opening clock position, distance between internal opening and anal verge, maximum track diameter, type of fistula (inter/trans/extra/supra sphincteric and superficial), presence of secondary branches, exit site location (gluteal, scrotal, vaginal, labial, urethral, blind ending with comment about right or left side), hyperintensity in T2W images, enhancement of tract, presence of abscess and any other specific additional findings (anovaginal fistula, rectal or sigmoid wall inflammation, Crohn's disease and prior surgeries).

Superior mesenteric artery syndrome (SMA syndrome) **Aorta: SMA distance** is reduced and measures ….. mm. **Aorta: SMA angle** measures …..^{O}, reduced. Compression of the D3 segment of duodenum between the aorta and SMA with over distension of the proximal duodenum and stomach. Left renal vein is compressed between the aorta and SMA. (Normal aorto-mesenteric angle measures 38–65 degrees. The normal distance from the aorta to the SMA at the duodenal crossing is 13–34 mm.)

Carcinoma prostate: Diffusion restricting T2 hypointense mass lesion in the bilateral mid and inferior, left lateral superior aspect of prostate with exophytic component noted on the left lateral aspect with infiltration of the left neurovascular bundles and bilateral seminal vesicles. On contrast, the lesion shows enhancement. Spectroscopy of the lesion shows elevated choline and decreased citrate. Multiple lymph nodes noted in the bilateral obturator and internal iliac regions. Bladder wall thickening—suggestive of chronic bladder outlet obstruction. Prostate measures 6 × 5 × 7 cm (vol 105 cc) enlarged in size. PSA density is 0.106 ng/ml/cm^3. Soft tissue lesion noted in the left superior pubic ramus—suggestive of secondaries: Features are suggestive of carcinoma prostate with extracapsular spread and bony and lymph node metastasis—PIRADS 5 (staging T4N2M1).

Benign prostatic hyperplasia: Prostate measures 5.6 × 5.4 × 5.2 cm (vol ~78 cc) enlarged in size, elevating the bladder base. Diffuse hyperintense central/transitional zone of prostate with multiple nodules. MR spectroscopy shows no elevation of choline/reduction of citrate. Diffusion weighted MRI imaging shows no abnormal restricted diffusion. Peripheral zone is uniformly hyperintense on T2 W images with no focal T2 hypointense lesion detected within. Peripheral zone is compressed. The T2 hypointense capsule is intact. No breech or focal bulge seen. The neurovascular bundle at 5 and 7 o'clock positions are normal. The angle between the seminal vesicle and prostate is maintained. The periprostatic fat plane is preserved. No stranding or infiltration seen. Seminal vesicles are normal in size. No T2 hypointense lesion noted within. No significant enlarged lymph nodes in the pelvis. No free fluid in the pelvis: Grade III prostatomegaly with benign prostatic hyperplasia.

Posterior urethral valve: High grade reflux into the right kidney with distended irregularly thickened bladder and marked dilatation of posterior urethra. Abrupt transition of dilated posterior urethra to small bulbous urethra with thin valve tissue extending from the ventral surface of the urethra—posterior urethral valve (Type I). No significant postvoid residual urine is seen. **Disproportionately dilated posterior urethra with an abrupt transition into a narrow anterior urethra—features could represent posterior urethral valve.**

Liver donor: Normal liver intensity with no focal/diffuse liver disease. Triple confluence pattern of the intraductal biliary anatomy (Type 2 pattern). Biliary ducts to segment IV joints the left hepatic duct 14 mm from the confluence of hepatic ducts. Conventional branching pattern of portal vein and hepatic vein.

Pelvic floor: Posthysterectomy status.There is widening of levator hiatus (transverse diameter), measuring 5.0 cm. H line (AP width of the levator hiatus) measures 7 cm at rest and 8.2 cm on straining—increased. Normal (<5 cm). M line (vertical descent of the levator hiatus) measures 1.1 cm at rest and 3.1 cm on straining—increased (normal<2 cm). Large cystocele noted: Part of the bladder is seen 3.1 cm below the PC line and 2.8 cm below the H line at rest, and 7.2 cm below the PC line on straining. Vaginal vault prolapse noted: Vaginal vault is seen 1.8 cm below the PC line at rest, 3 cm below the PC line on straining. The distance of the pubococcygeal line to the anorectal junction on rest is 1.1 cm below PC line at rest and 3.2 cm on straining—mild rectal prolapse. Herniation of fat between the vagina and rectum at rest and exaggerated on straining. No evidence of descent of small bowel loop between vagina and rectum to suggest enterocele. There is significant caudal inclination of the levator plate on rest (19°) and exaggerated on straining—63 to PC line (anorectal angle normal 90° to 110°). The levator ani muscle is mildly thinned and show normal signal intensities.

There is significant posterior perineal descend on straining and during defecation. M line (vertical descent of the levator hiatus) measures 4 cm at rest and 6.5 cm on straining— significant increased descent (normal <2 cm). Moderate descent of rectum through the levator hiatus. There is anterior rotation of urethra into horizontal plane in the dynamic images—anterior hypermobile urethra. Mild anterior rectocele, measures 2.1 cm anterior to the expected location. Significant caudal inclination of the levator plate on straining–61 degrees to PC line (normal <10 degrees). Transient rectal intussusception on straining. Anorectal angle on straining at rest measures 110°, squeezing 85 and on straining 140°.

Defecogram: Moderate anterior rectocele, measures 4.3 cm anterior to the expected location. No evidence of rectoanal intussusception. Anorectal angle at rest is 90 . During straining 130°.

Patient not able to empty the rectal jelly on evacuation phase. No evidence of rectocele, abnormal descent/rectal intussusception/enterocele. However, possible milder form of pelvic dyssynergia cannot be ruled out.

Anterior rectocele noted on straining and evacuation stage, measures about 2.4 cm. Defecography done at rest, during maximal sphincter contraction (squeezing), during straining, and during defecation. Anorectal angle (ARA), the angle between the two lines that intersect at the ARJ, 121. During squeezing (maximal pelvic floor contraction), there is elevation of the pelvic organs in relationship to the PCL and sharpening of the ARA (due to contraction of the puborectal muscle) by 15–20. During straining and defecation, the pelvic floor muscles relaxes and, therefore, a mild descent (<2 cm) of the pelvic organs is noted. In addition, the anorectal angle becomes more obtuse, typically 15–20 more than when measured at rest. During defecation, the anal canal opens and the contrast material is evacuated. No e/o rectal intussusception/prolapse. The levator ani muscle focal thinning on right side.

Renal

Autosomal dominant polycystic kidney disease: Multiple simple bilateral renal cortical cysts are seen. There are multiple (~…) cysts of varying sizes in left kidney (largest measuring ……..cm). There are ~ … cysts of varying size in the right kidney, the largest one measuring ….cm. The right kidney measures ….cm. The left kidney measures ….cm. Both kidneys are enlarged in size. No calculus or caliectasis is seen on either side. Ureters are not dilated. Multiple cysts in liver predominantly in the left lobe of liver. Above features favor autosomal dominant polycystic kidney disease.

Vesicoureteric junction calculus: 6 mm calculus in the left vesicoureteric junction causing mild hydroureteronephrosis. Mild delayed excretion noted. Another 3 mm seen calculus just above the calculus. CT attenuation value of the calculus is + 565 HU.

Pelvic ureteric junction obstruction: Grossly dilated left renal pelvis [6.6 cm (AP)] and mild dilatation of left calyces with partial left pelvic ureteric junction obstruction. Accessory left renal artery indenting on the posterior aspect of left PUJ. Delayed imaging shows contrast in the left renal pelvis. Narrowed segment of left PUJ and upper ureter measures 12 mm in length contrast noted in the left ureter in delayed images.

Wilms tumor: …..size well-defined mass lesion in the anterior aspect of lower pole and interpolar region of right kidney. The lesion is supplied by a prominent arterial feeder from the right renal artery. The right main renal artery courses the above the mass. There is a non-occluding tumor thrombus involving the right renal vein and extending to the infrahepatic suprarenal portion of IVC for a length of …. mm. Delayed images show, persistent nephrogram with non-opacified dilated right renal pelvic calyx cyst.

Table 2.16: Renal measurements reporting format

Cortical thickness	*Right kidney*	*Left kidney*
Upper pole	25 mm	19 mm
Interpolar region	18 mm	16 mm
Lower pole	18 mm	18 mm

Pyelonephritis: Right kidney appears enlarged and globular with perinephric fat stranding and thickening of anterior and posterior pararenal fascia noted. No focal collection/air pockets/calculi.

Emphysematous pyelopheritis: Right kidney measures cms, normal size. Left kidney measures cm, mildly bulky. Urothelial thickening on left side with perinephric and periureteric fat stranding. Minimal air seen in upper pole/interpole calyx of left/right kidney. No intraparenchymal air. Presence/absence hydroureteronephrosis. No renal/perirenal abscess on plain scan. Bladder is partially distended with mild diffuse wall thickening. Minimal air seen in nondependent bladder lumen.

Renal cell carcinoma: Well-defined heterogeneously enhancing >50% exophytic mass lesion measuring 3.4 × 5 cm noted in the posterior surface of lower pole of right kidney which is 10 mm away from the hilum. The lesion shows no contact with renal vessels. No evidence of renal vein thrombosis/para aortic lymphadenopathy/perinephric extension. Visualised bones appear normal. Areas of non enhancing hypodensity noted within the mass suggestive of necrosis. **Renal nephrometry score-4. (T1bN0M0).**

Renal carcinoma checklist: Mass size, growth rate (interval scan), type of mass (cystic/solid/indeterminate), presence of fat, enhancement pattern, location, mass margins, capsular location (50% exophytic, <50% exophytic, endophytic), distance to the sinus fat or collecting system. Tumor thrombus (distal extent) [no tumor thrombus/ipsilateral renal vein (no IVC extension)/IVC below diaphragm/IVC above diaphragm/into right atrium], bland venous thrombus, lymph nodes and metastases in field of view.

Adrenal lesion: Table 2.16.

Renal Donor Angiogram

Right side: Right kidney is normal size, shape position and axis. It measures 10.4 × 5.2 cm. **Moderate perinephric fat seen.** No evidence of mass lesion or hypoperfusion is visualized. No evidence of tumor/cyst/calculus/angiomyolipoma. Right ureter is normal.

Table 2.17: Adrenal lesion metrics reporting format		
Parameter	*Right adrenal lesion*	*Left adrenal lesion*
Size	52 (CC) × 31 (TR) × 31 (AP) mm	36 (CC) × 21 (TR) × 18 (AP) mm
Morphology	Irregular, heterogeneous enhancement	Heterogeneous enhancement with central necrosis
Unenhanced CT HU	27 HU	27 HU
Enhanced CT HU value (60 sec, portal venous phase)	80 HU	60 HU
Delayed enhancement CT HU value (10 to 15 mins)	58	35
Absolute washout: (enhanced CT-delayed CT)/(enhanced–unenhanced CT) × 100		
>60% suggestive of adenoma	22/53 = 41%	25/33 = 75%
Relative washout: (enhanced CT-delayed CT)/(enhanced CT) × 100		
>40% suggestive of adenoma	22/80 = 27%	25/60 = 41%

Left side: Left kidney is normal size, shape position and axis. It measures 9.1 × 5 cm. **Moderate perinephric fat seen.** No evidence of mass lesion or hypoperfusion is visualized. No evidence of tumor/cyst/calculus/angiomyolipoma. Left ureter is normal.

Single ureters on both sides. Adrenals are normal. No evidence of congenital anomalies noted in both the kidneys and ureter.

Abdominal angiogram and both lower limb angiogram: ***Right side:*** Eccentric thrombus with filling defect in the distal right common iliac extending to external iliac artery of approximate length 4.7 cm (narrowing by 70–80%) with peripheral flow. Common iliac artery diameter above occlusion is 8 mm. Common femoral artery below occlusion is 7 mm. Total occlusion of popliteal artery of approximate length is 12.5 cm with minimal reformation of mid anterior tibial and peroneal artery through collaterals. Popliteal artery above the occlusion measures 4.3 mm in diameter. Narrowing and occlusion of distal anterior tibial artery. No flow in the posterior tibial artery.

Left side: Common iliac, common femoral, superficial femoral, deep femoral and popliteal arteries appear normal. Popliteal trifurcation, anterior, posterior tibial and peroneal artery appear normal.

Infrarenal abdominal aorta aneurysm: There is large infrarenal fusiform aortic aneurysm [55 (TR) × 55 (AP) × 83 mm (length)] with peripheral eccentric thrombus, measuring about 21 mm (AP) × 49 mm (ML) in maximum dimension and 92 mm (CC) in the inferior and lateral walls, distal 1.5 cm of infrarenal abdominal aorta and aortic bifurcation appear normal. Peripheral calcification noted. Renal arteries origin seen just above the upper end of aneurysm and appear normal. No evidence of dissection/intramural hematoma noted. No periaortic inflammation/hematoma noted. Maximum diameter of contrast filled lumen measures 46 × 34 mm. Focal complete occlusion of inferior mesenteric artery. Both common iliac arteries appear normal except mild atherosclerotic changes. Mild osteal and juxtaosteal segment narrowing of left accessory renal artery.

Musculoskeletal System (MSK)

Dislocation of AC joint: Grade 3 injury of right acromioclavicular joint (complete dislocation of AC joint) with complete tear of superior and inferior acromioclavicular ligaments, complete tear of conoid and trapezoid components of coracoclavicular ligament, grade 1 sprain of deltoid and trapezius muscles.

Brachial plexus palsy: Muscles atrophy with increase signal intensity noted in the entire right arm and shoulder muscles. Complete preganglionic avulsion of the right C8 nerve root with pseudomeningocele formation. Retracted thickened C8 nerve root is seen just lateral to the neural foramina. Thickened extra neural foramen portion of right C5, C6 and C7 nerve roots upper and middle trunk forming a ill-defined soft tissue in the right interscalene triangle and minimally extending to the right costoclavicular space (retraction ball). Ill-defined lobulated soft tissue is at the level of divisions and possibility of neuroma formation with adjacent soft tissue fibrosis. Division and cords of the right brachial plexus appear normal. T1 nerve root relatively appears normal (Table 2.19).

Glenohumeral dysplasia following obstetric brachial plexus injury: Posterior subluxation of left shoulder joint (percentage humeral head anterior to the scapular line is 28.5%). Hypoplasia of the mid and inferior glenoid especially posteroinferior part of the glenoid. Glenoid is convex and showing posterior sloping. Glenoscapular angle is 12 degrees. Glenoid retroversion noted (13 degrees). Left scapular width measures 43.0 mm. Right scapular

Table 2.18: Donar renal artery measurements sample format				
Renal artery	*Right*		*Left*	
Number	Single		Single	
	Main	*Accessory*	*Main*	*Accessory*
Length—distance between origin and 1st segmental bifurcation	33 mm			17 mm
Distance between the IVC margin and the 1st segmental bifurcation	9.8 mm		NA	NA
Orthogonal diameter	4.2 mm		5.0 mm	
Origin at the level of	D12-L1 vertebrae level		Upper border of L1	
Branching (hilar/polar/capsular)	Superior polar		Hilar	
Stenosis or aneurysm				
	Evidence of early branching like branching occurs < 1 cm from the right IVC margin		No evidence of left early segmentary arterial branching (segmental branching <1.5 cm from the origin of left renal artery.)	

Table 2.19: Donar renal vein measurements sample format				
Renal vein	Right		Left	
	Main	Accessory	Main	Accessory
Length—segmental confluence to IVC	mm	mm	mm	
Segmental confluence of left renal vein to left margin of aorta	NA	NA	mm	
			No evidence of retroaortic/circum aortic renal vein	
	No evidence of late segmental confluent (<2 cm from the right side of IVC)		No evidence of late segmental confluent (<2 cm from the left margin of aorta)	
Diameter	mm	mm	mm	
Origin at the level of	L1–L2		L1 vertebrae	
Aneurysm				
Renal vein tributaries	No tributaries		Left adrenal vein Inferior phrenic Left gonadal vein (<5 mm) Lumbar vein (< 5 mm)	
			No abnormal venous drainage of segmental renal veins into lumbar, hemiazygous veins.	
Thrombosis				

width measures 42.3 mm. Left scapular length measures 77.6 mm Right scapular length measures 58.7 mm. Left humeral head appears smaller and flattened.

Hill-Sachs and bony Bankart lesion: Moderate Hill-Sachs impaction fracture of the posteriosuperolateral humeral head measuring 21 (AP) mm × 6 (depth) mm.Tear of the anteroinferior labrum from 3 to 6 o'clock position with fracture of the underlying glenoid—bony Bankart lesion. There is avulsion of IGHL labral complex from the glenoid (2–6 o'clock position) with periosteal stripping (soft tissue Bankart variant—ALPSA: Anterior labroligamentous periosteal sleeve avulsion). Small bony fragment measuring 10 × 4 mm adherent to the inferior glenoid at 6 o'clock position. No significant bony loss in the anteroinferior glenoid.

1. Hill-Sachs interval …… mm
2. Nonengaging, on track Hill-Sachs defect/engaging, off track Hill-Sachs defect.

Adhesive capsulitis: Thickened oedematous inferior glenohumeral ligament, axillary pouch of inferior capsule and rotator interval. Fluid distension of biceps tendon sheath—features suggestive of adhesive capsulitis.

Comminuted impacted fracture neck of humerus extending into head with displaced superiorly migrated greater tubercle and inferomedially rotated humeral head. Greater tubercle containing the insertion of the supra and infraspinatus tendon. Displaced inferior aspect of lesser tubercle. Tiny displaced bony fragment noted in subscapularis bursa.

Rotator cuff tear: Irregular partial thickness tear of foot print of supraspinatus tendon involving ~70% thickness, anteroposterior extend of 18 mm, maximum retraction of ~8 mm extending to bursal surface. No muscle atrophy.

Bursal surface partial thickness tear of the foot print of anterior supraspinatus tendon measuring about 7 mm (Trans) × 10 mm (AP) involving ~ 70% thickness. No evidence of musculotendinous retraction/atrophy noted.

Linear intrasubstance partial thickness tear (~60% thickness) of anterior foot print of the supraspinatus tendon measuring about 6 mm (Trans) × 13 mm (AP). No evidence of musculotendinous retraction/atrophy noted.

Full thickness tear of supraspinatus tendon measuring about 15 mm (Trans) × 20 mm (AP) with moderate fatty atrophy of supraspinatus muscle. Full width, full thickness tear of the supraspinatus tendon with significant retraction of ~3.5 cm. Retracted end is irregular and seen at medial humeral head level. Mild fatty atrophy of supraspinatus muscle.

TFCC tear on the ulnar styloid attachment with fluid extending along the base of the TFCC and surrounding the styloid. Evidence of well-defined elongated cystic lesion measuring about 30 × 12 × 16 mm along the dorsal aspect of the distal ulna, extending into the ulnar side of the TFCC.

Ganglion cyst: Well-defined lobulated cystic lesion (1.8 × 0.5 × 0.7 cm) noted in the palmar aspect of the wrist ulnar side, seen behind the flexor carpi ulnaris tendon and communicating to the ulnotriquetteral joint space. No e/o ulnar artery/nerve compression.

Full thickness tear of the ulnar collateral ligament (UCL) of the 1st meta carpophalangeal joint with cortical irregularity of the proximal phalanx. Complete tear of the ulnar collateral ligament of the first metacarpophalangeal joint with proximal retraction and displacement—**Stener lesion.**

Carpal tunnel syndrome: Mild cross sectional enlargement and hyperintensity of median nerve deep to flexor retinaculum. Flattening of the median nerve at the level of hamate with oedema. Palmar bowing of flexor retinaculum at the level of hamate. No evidence of flexor tendon tenosynovitis. Mild hyperintensity in thenar muscles.

de Quervain tenosynovitis: Mild thickening and increase signal intensity of abductor pollicis longus and extensor pollicis brevis and fluid distension of tendon sheath.

AV fistula: Left radiocephalic AV fistula noted with intact anastomosis, flow across AVF measures more than 500 ml/min. Thrombotic occlusion noted in the cephalic vein in the upper forearm with reversal of venous flow towards the wrist. Deep veins appear normal. A few tiny veins in the palmar aspect of the forearm draining into the deep veins. Cephalic and basilic veins around the cubital fossa contracted on both sides. Deep veins and arteries of the both upper limbs appear normal.

Table 2.20: Brachial plexus reporting format

	Pre-ganglionic nerve root	*Post-ganglionic*	
		Nerve roots and trunk	*Divisions and cords*
C5	Intact. No evidence of nerve root avulsion of pseudo-meningocele	Thickened proximal C5 and C6 nerve roots with and retracted upper trunk suggestive of rupture.	Ill-defined lobulated soft tissue is at the level of divisions and possibility of neuroma formation with adjacent soft tissue fibrosis.
C6	Intact. No evidence of nerve root avulsion or pseudo-meningocele		
C7	Rupture with evidence of nerve root avulsion/pseudo-meningocele	Middle trunk could not be traced separately from the abnormal soft tissue at the level of divisions and proximal cords	
C8	Intact. No evidence of nerve root avulsion or pseudo-meningocele	Post-ganglionic nerve root appear normal. Lower trunk could not be traced separately from the abnormal soft tissue at the level of divisions and proximal cords	
D1	Intact. No evidence of nerve root avulsion or pseudo-meningocele		

Osteoarthritis: Patellofemoral and medial tibiofemoral osteoarthrosis with reduction of medial tibiofemoral joint space, full thickness loss of patellar facet, trochlea and medial condylar cartilage, subchondral sclerosis with marrow oedema in the patellar, trochlea medial femoral condyle and medial tibial plateau. Degenerative changes of the medial meniscus. Tear of posterior root attachment of medial meniscus with extrusion of body into the medial joint recess, 3.5 mm beyond the margin of medial tibial plateau. Moderate mucoid degeneration of anterior cruciate ligament. No tear. Degenerative subchondral marrow changes in the median, tibial eminence.

Chondrosarcoma: Lytic destructive lesion with irregular sclerosis in the medial aspect of left iliac bone with adjacent soft tissue. It measures ~6.1 × 7.1 cm. Destruction involves the iliac articular surface of the left SI joint. There is mild smooth erosion of the adjacent sacrum with minimal marrow edema.

Ewing's sarcoma: X-ray: Irregular cortical thickening with areas of minimal cortical destruction and lamellated periosteal reaction with mild soft tissue component noted in the diaphysis of right humerus.

Osteosarcoma: **X-ray**—ill-defined lytic lesion approximately measuring noted in the metaphysis of distal femur with osteoid matrix, wide zone of transition with aggressive periosteal reaction, adjacent large soft tissue component noted with multiple specs of calcification/ossification noted. An ill-defined lucent lesion involves the metaphysis and distal diaphysis of the femur. It does not appear to reach the growth plate. Laterally the mass elevates the cortex with periosteal reaction.

***Osteosarcoma MRI*:** A right lower femoral shaft metadiaphyseal osteolytic exophytic lesion is seen showing a wide zone of transition with the adjacent normal bone marrow and encasing the posterolateral circumference of the distal femoral shaft. The lesion elicits inhomogeneous isointense T1/T2 and high STIR signals with internal break-down foci of fluid signal. The lesion causes cortical destruction with and extraosseous eccentric soft tissue component measuring 9.1 × 8 × 7.7 cm in orthogonal dimensions. The lesion and the soft tissue component show heterogeneous contrast enhancement. The quadriceps femoris muscle (mainly the vastus lateralis muscle) shows signal changes and post-contrast enhancement similar to the lesion and appears stretched over the lesion/edema of the popliteus, proximal tibialis anterior and posterior muscles. No other lesions in the scanned bones or invasion of the popliteal neurovascular bundle. No obvious extension of the lesion to the physis/epiphysis.There is mild overlying soft tissue thickening. No soft tissue abscess collection.

Ill-defined mass lesion noted in the intramedullary aspect of the lower end of femur in metaphyseal-diaphyseal region with cortical breach in the medial aspect, interrupted periosteal reactions, minimal extra osseous soft tissue component and areas of hemorrhages. The lesion appears to involve the growth plate with minimal involvement of epiphysis. On dynamic contrast, the soft tissue component showing well enhancement in arterial phase with washout on delayed imaging—consistent with high grade neoplasm. Minimal surrounding nonenhancing edema seen. Coronal height of lesion measures 10 cm. Upper limit of lesion seen 13 cm from the femoral articular surface. No evidence of joint effusion. No other skip lesion in the rest of the femur. No evidence of neurovascular bundle involvement.

Femoroacetabular impingement (pincer type): Ossification of superolateral acetabular labrum on both sides, leading to over coverage of femoral head. No acetabular retroversion. Herniation pit noted in anterior femoral head-neck junction on left side. The femoral head neck junction is smooth and concave on both sides. No evidence of any dysplastic bump in the femoral head. No marrow edema. Alpha angle measures 41 degrees on left side, normal.

Femoroacetabular impingement (pincer type): Loss of weight bearing articular cartilage of left hip with subchondral cyst in the acetabulum. Mild left hip joint effusion. Decreased extrusion index –9% (25% in normal subjects). Decreased extrusion index suggests femoral head becomes "more covered". No evidence of femoral head, neck junction offset/bump. α angle measures about 45 (abnormal - >50 degree).

Femoroacetabular impingement (cam type): Alpha angle on the right and left side measures about 64 and 54 degrees, respectively (normal <60′ degree). Lateral capsular thickening with irregularity noted in the right side. A bump in noted head and neck junction.

Perthes' disease: Left capital femoral epiphysis appears flattened with altered signals and subchondral fractures. Overlying the femoral head, articular cartilage appears intact. Altered marrow signal abnormality extending to the femoral neck. Acetabulum appears normal.

Developmental dysplasia of hip: Bilateral developmental dysplasia of hip with superior dislocation. Bilateral shallow acetabulum with deficient posterior and superior acetabular rim (Table 2.20).

Post-DDH reduction hip joint: Right DDH. Right femoral head is seen within the acetabular cavity.

Acetabulum is shallow and femoral head is small on right side. Edema of soft tissue around right hip joint. No evidence of bony destruction identified. Remaining underlying bones including the neck and upper shaft of the femur appear normal bilaterally. Right femoral head ossified epiphysis appears mildly smaller in size. Post-surgical changes in the right inguinal region and upper medial aspect of thigh.

Avascular necrosis: Avascular necrosis with multiple subchondral crescent fractures leading to minimal collapse of articular surface of femur head on right side. It involves about 60–70% of femur head. No secondary osteoarthritis. No right hip joint effusion. Avascular necrosis with multiple subchondral crescent fractures leading to significant collapse and deformity of femur head on left side. There is secondary osteoarthritis with articular margin irregularity of the acetabulum and marginal osteophytes. Mild left hip joint effusion. Avascular necrosis of bilateral femoral heads—modified Ficat Arlet stage III on right side and stage IV on left side.

Idiopathic chondrolysis of hip: Geometric T1 hypo T2 hyperintense signal intensity alteration in the mid one-third of proximal right femoral head. No obvious evidence of hip joint effusion/synovial thickening/acetabular oedema—features suggestive of idiopathic chondrolysis of hip.

Odelberg disease: Oedema in the left inferior pubic ramus—van Neck-Odelberg disease.

Anterior cruciate ligament graft: The tibia tunnel is in the anterior third of the tibial plateau mildly anterior to the Blumensaat's line on sagittal images with the tunnel opening through the medial tibial eminence in the coronal images.The distal tibial tunnel measures 13 mm and the tibial opening measures 7 mm. The graft in the tibial tunnel shows hyperintense amorphous signals—suggestive of mucoid degeneration.

Graft in the intercondylar notch: The graft in the intercondylar notch shows hyperintense amorphous signals and buckling—suggestive of graft degeneration. No spurs along the intercondylar roof. T2 dark soft tissue noted in the anterior intercondylar notch anterior to the ACL fibres. Post-operative scar in the Hoffa's fat pad leads to this above-mentioned lesion. Ill-defined synovial soft tissue noted in the intercondylar notch with a metallic artefact (suture material) in the proximal intercondylar notch.

Table 2.21: DDH sample reporting format

Structure	*Size*	
	Right	*Left*
Femoral head (bone) epiphysis	10 × 12 × 6 mm	10 × 10 × 7 mm
Femoral head (cartilage) epiphysis	25 × 10 mm	21 × 9 mm
Greater trochanter (bone)	8.5 × 10.8 mm	8 × 10.9 mm
Greater trochanter (cartilage)	20 × 19 mm	21 × 20 mm

Femoral tunnel: The femoral tunnel is at the intersection of the physeal scar and the Blumensaat's line posterior to the line along the posterior femoral cortex. The femoral tunnel is at the 1 o'clock on coronal images. Femoral tunnel measures 10 mm. The graft in the femoral tunnel shows mild hyperintensity on T2-weighted sequence.

Intrameniscal degeneration of medial meniscus with radial tear of the posterior root attachment and partial extrusion of the body into the medial joint recess, 3 mm beyond the margin of medial tibial plateau.

Meniscal contusion in the posterior horn–posterior body junction of medial meniscus with tiny vertical tear in the peripheral third (red zone) of tibial articular surface.

Chondromalacia patella: Patella shows fraying of articular cartilage with multiple defects that involves less than 50% surface. Increased signal intensity in cartilage is noted, no evidence of edema in bone—chondromalacia patella grade 2.

Osgood-Schlatter disease: T2/ PD shows thickening and edema in distal patellar tendon. Bone marrow edema is noted in patellar tuberosity. Distended deep infrapatellar bursa noted. Soft tissue swelling noted anterior to tibial tuberosity.

Neurofibroma: Multilobulated solid lesion in the left forearm in the upper third, mid-third junction. The lesion shows continuity with the median nerve. The lesion is extending up to the subcutaneous plane in the upper forearm. The lesion shows a few fibrous septa. The lesion shows diffusion restriction—**features favours neurofibroma in the left median nerve.**

Exostosis: Pedunculated exostosis arising from the lower end of femur medial aspect measuring about 2.1 × 2.2 × 4 cm. Cartilage cap thickness measuring about 9 mm. No evidence of bursitis/no evidence of fracture/no significant muscle altered signal intensity**.**

***Blount's disease*:** Absent medial most bony epiphysis with adjacent depressed metaphysis which has beak-like protuberance. There is tibial varous deformity. No evidence of bony physeal bar—features favour Blount's disease.

Transient lateral patellar subluxation with bone marrow oedema in the medical patella and lateral condyle of femur. Grade I sprain of medial patellar retinaculum at patellar attachment and grade I strain of vastus medialis oblique muscle. No evidence of osteochondral injury/bone marrow oedema in the inferomedial aspect of patella. Complete tear of medial patellofemoral ligament and medial patellar retinaculum at the femoral attachment. Grade I strain of vastus medialis oblique muscle and tendon.

Insall–Salvati ratio = patellar tendon/patellar length: 4.5/3.9 = 1.44 (patella alta).

Patellar tilt: Lateral patellofemoral angle opens medially (70) – abnormal (positive for patellar tilt). Suggest patellofemoral malalignment. Patellar apex lying lateral to the plane of trochlear apex—patellar subluxation. Patellar congruence angle is positive suggestive of patellar subluxation. **Congruence angle:** Angle of congruence is an index of subluxation but does not assess tilt. If congruence angle is lateral to congruence line, then angle is positive.

If congruence angle is medial to congruence line, then angle is negative. Normal angle is ≤16°. Sulcus angle: **Establish a zero reference line. Normal sulcus angle is** ≤135 ± 10°.

Q angle – normal <15°, abnormal >20–25°

Patellofemoral malalignment

Type I—Patellar subluxation (displacement) without tilt.

Type II—Patellar subluxation with tilt.

Type III—Patellar tilt without subluxation.

Tibial tuberosity—trochlear groove distance is 20 mm. (>20 suggest lateralized tibial tubercle).

Femoral ante version—measurement.

Bump (nipple) in the anterosuperior femoral trochlea–suggestive of femoral trochlear dysplasia. No evidence of crossing sign in X-ray lateral view.

Trochlear articular facet asymmetry. Medial to lateral facet ratio—(0.67, normal) <0.4, abnormal. Degree of patellar lateralization (patellar lateralization more than 6 mm is significant).

Patellar Wiberg morphology

Wiberg I: Medial and lateral facets are concave and identical. Wiberg II: Medial facet is concave and narrow. Lateral facet in concave. Wiberg III: Medial facet is convex and narrow. Lateral facet is concave. Wiberg IV: Medial facet is flat and narrowed.

Patellar tracking; Comparison of static and dynamic study of the knee joint to assess the change in patella related to the femur during knee flexion and extension known case of **patellofemoral instability,** CT and MRI screening show. Avulsion fracture of the medial patellar retinaculum at patellar attachment and grade 2 strain at medial attachment.Widely placed tibial tubercle (TT distance measures about 2.1 cm on left, 2.4 cm on right). Borderline patellar alta. No significant trochlear dysplasia except tiny bony hump in midline.

***Patellar tendon lateral femoral condyle friction syndrome*:** Focal area of high T2 signal (oedema) at the inferolateral aspect of the patellofemoral joint, within the superolateral portion of the infrapatellar (Hoffa's) fat pad—patellar tendon lateral femoral condyle friction syndrome. No evidence of patella alta.

Ligament injury: Proximal medial collateral ligament appear thickened and hyperintense with bone marrow edema noted in medial femoral epicondyle. Posterior oblique ligament, ACL, medial and lateral meniscus and other ligament appears normal—grade 2 **medial collateral ligament injury**.

ACL: Anterior cruciate ligament appears hyperintense with a fluid signal noted at the femoral intercondylar notch. ACL angle appears normal and measures 12°. Hyperintensity noted in the lateral femoral condyle. Proximal MCL appears hyperintense—partial tear of medial collateral ligament.

Post-operative ACL reconstruction: ACL reconstruction status intact without tear. Increased signal intensity noted in the ACL graft.

Lateral collateral ligament: Hyperintensity noted in the lateral collateral ligament, the distal continuity of the ligament not maintained, chip fracture involving fibular head noted. Hyperintensity in popliteus tendon and popliteofibular ligament noted. Other posterolateral corner structures appear uninjured, no meniscal tear, medial collateral and cruciate ligament appear to be intact—**chip fracture in fibular head with a complete tear of lateral collateral ligament.**

***Posterior cruciate ligament*:** Hyperintense posterior cruciate ligament noted with AP diameter on sagittal T2 weigted images measures 12 mm. Bony contusion in tibial plateau noted. Medial collateral ligament appears hyperintense–grade 1 strain. Joint effusion noted—posterior cruciate ligament tear with grade 1 strain on posterior cruciate ligament.

Meniscal tear: Longitudinal tear of the body and posterior horn of medial meniscus, no extrusion or parameniscal disc formation. Lateral meniscus appears intact. Collateral and cruciate ligaments appear normal, no bone marrow edema.

***Bucket handle tear of medial meniscus*,** with flipped fragment in intercondylar notch anterior to posterior cruciate ligament giving double PCL appearance.

The flipped fragment is attached to parent meniscus anteriorly and posteriorly.

Congenital talipes equinovarus (CTEV): Talipes varus deformity noted. No obvious tarsal coalition. No evidence of vertical talus. Mild laterally angulated talus. Muscle mass appears small. Increased subcutaneous fat noted (OR) Mild fatty atrophy of the distal leg and plantar muscles. Mild reduction of tibiotalar joint space.

Plantar fasciitis: Thickening with increased signal intensity of the medial cord of the plantar aponeurosis with marrow edema of the underlying calcaneum and significant perifascial inflammation. Moderate size plantar calcaneal spur noted.

Morton's neuroma: Ill-defined T1 hypointense lesion measuring about 8 × 4 mm noted in the plantar soft tissues in between 2nd and 3rd metatarsal head with surrounding areas of T2 hyperintensity with edema extending into the dorsal aspect of the foot.

Os calcaneus secundarius: Well-defined ossification adjacent to the anterior process of calcaneum without marrow edema.

Bilateral congenital vertical talus: Bilateral congenital vertical talus. No obvious evidence of talo calcaneal/calcaneo navicular coalition.

Haglund's deformity: Increased thickness of distal Achilles tendon with altered signal intensity at the insertion (Insertional Achilles tendinitis) with calcaneal bony prominence, adjacent Calcaneal oedema and retro calcaneal bursitis.

Mechanical axis of the right lower limb (genu valgum) measuring about 10 degrees.

Obstetrics and Gynaecology

Follicular Study (TVS)

Baseline study on the day of first examination (Table 2.21):

- *Uterus:* Measures 6.7 × 4.3 × 3.1 cm. Uterus is anteverted and anteflexed in position. It appears normal in size and echotexture. Its surface appears normal without any contour abnormality. No myometrial focal lesion is seen. Cervix also appears normal.
- *Right ovary:* 3.1 × 1.5 cm
- *Left ovary:* 2.9 × 1.7 cm. Both ovaries are normal in size, shape and echotexture. Uterine artery PI measures 2.6 on right and 2.3 on left side, suggesting favourable outcome (<3 favourable outcome, >3 less favourable outcome, even with PCOD) (Uterine PI reduces up to 1, near ovulation).
- *Adnexae:* No adnexal mass lesion is seen.

Common measurements in lower limb

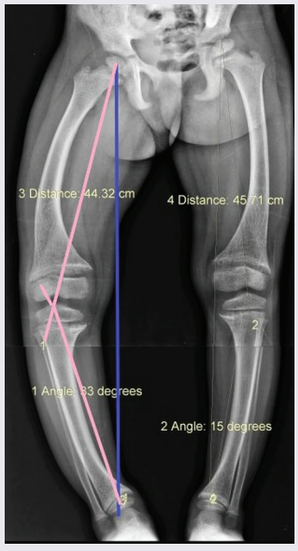

Fig. 2.9: Mechanical axis–varus deformity
The mechanical axis should pass just medial to the center point of the knee joint. If the line passes more medially to the knee center, a varus deformity is present; if the line passes laterally to the knee center or center of the distal femur, a valgus deformity exists

1. The mechanical axis of the lower limb (blue line) is determined on the full-length AP standing radiograph. The axis passes through the center point of the hip joint (center of the femoral head) and through the center point of the ankle joint (midpoint of the tibial plafond).
2. Mechanical axis of the femur (MAF): A line from the center of the femoral head to the center of the distal femur or center of the knee (upper pink line)
3. Tibial shaft axis and mechanical axis of the tibia: A line extending from the center of the proximal tibia to the center of the ankle (lower pink line)
4. Mechanical axis of femur and tibia forms the lower limb valgus / varus angle

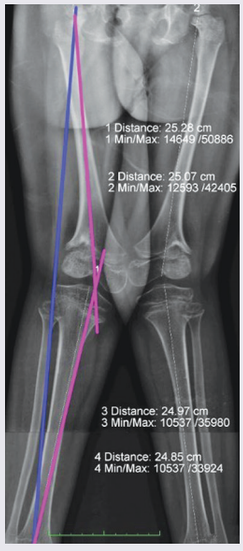

Fig. 2.10: Mechanical axis—valgus deformity

1. Insall–Salvati Index: The Insall–Salvati index is used for measuring the vertical position of the patella. The greatest diagonal length of the patella (LP) is measured from its posterosuperior corner to the apex. The length of the patellar tendon (LT) is measured from the patellar apex to the tibial tuberosity. The ratio of these two measurements (LP/LT) is the Insall–Salvati index

- Normal range: LP/LT = 0.8–1.2
- High-riding patella (patella alta): LP/LT <0.8
- Low-riding patella (patella baja): LP/LT >1.2

Fig. 2.11: Insall–Salvati index

2. Lateral patellofemoral angle of Laurin–The lateral patellofemoral angle is determined by drawing a line tangent to the highest points on the medial and lateral femoral condyles (A) and drawing a second line (B) across the lateral patellar facet. In a normal joint, these lines will typically form an acute angle that opens on the lateral side. In patients with patellar instability, the lines will often be parallel or may even form an angle that opens on the medial side. Figure Lateral patellofemoral angle opens medially (7°)–abnormal (positive for patellar tilt).

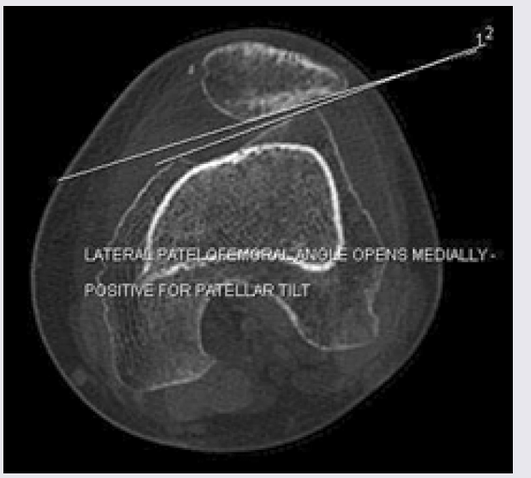

Fig. 2.12: Lateral patellofemoral angle of Laurin

3. Sulcus angle—measured by drawing the following lines. The deepest point of the trochlea is identified (A), and the highest points on the medial (B) and lateral femoral condyles (C) are marked. The angle formed by lines AB and AC is the sulcus angle. Normal sulcus angle is <– 137 degrees

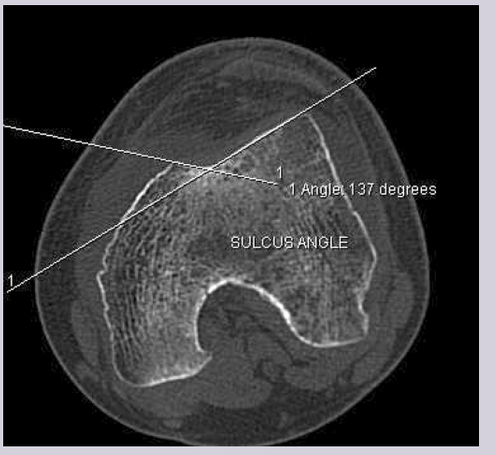

Fig. 2.13: Sulcus angle

4. The congruence angle of the patellofemoral joint—first identify the sulcus angle. The bisector of that angle is drawn as reference line. Another line drawn by joining sulcus and lowest point of patellar articulating surface. The angle between these two is the patellofemoral congruence angle. If second line is medial to first line, the angle has a negative value; if second line is lateral to first line, the angle is positive. Angle of congruence is an index of subluxation but does not assess tilt. Normal angle is <–16 degrees. Angles greater than +16° denote lateral subluxation of the patella.

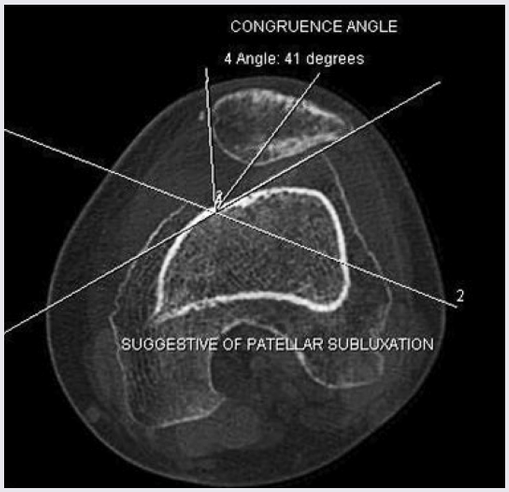

Fig. 2.14: Congruence angle of the patellofemoral joint

5. Trochlear depth: This measures the inset depth of the trochlear groove (sulcus) relative to the average of the maximum anteroposterior distance of the medial and lateral femoral condyles (it is determined on axial images at the same level as trochlear facet asymmetry). Trochlear groove depth < or = 4 mm is normal.

Fig. 2.15: Trochlear facet asymmetry

6. Medial to lateral facet ratio: The ratio of the medial facet length divided by the lateral facet length. <0.4 is abnormal indicates trochlear dysplasia.

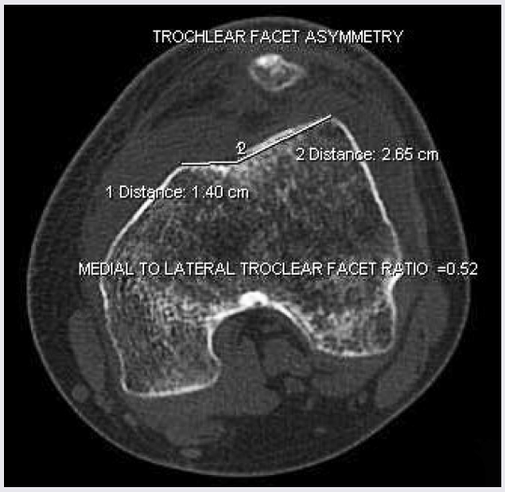

Fig. 2.16: Trochlear dysplasia

7. Lateralization of the patella: This evaluates the lateral patellar displacement, measuring the distance between the lateral margin of the trochlea and the most lateral point of the patella. A distance greater than 6 mm is indicative of trochlear dysplasia.

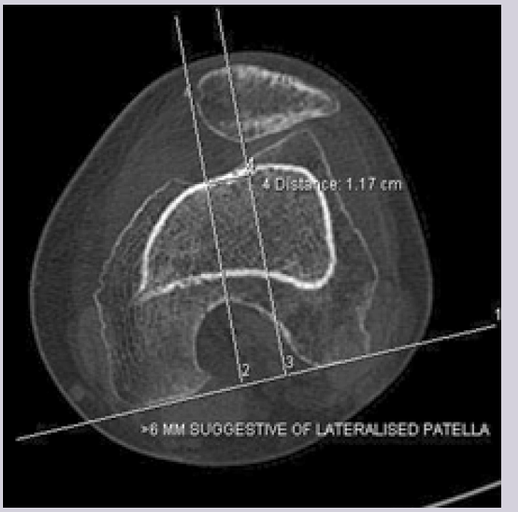

Fig. 2.17: Trochlear dysplasia

8. Lateralization of the tibial tuberosity: The position of the tibial tubercle is crucial for the inferolateral force vector of the patella. If there is excessive lateralization of the tibial tuberosity, the patella is pulled laterally during flexion. Therefore, excessive lateral displacement of the tibial tuberosity is a risk factor for lateral patellar dislocation. Imaging techniques are the only accurate way to measure the tibial tuberosity to the trochlear groove (TT-TG) distance. The distance from the tibial tuberosity to the trochlear groove (TT-TG) is measured parallel to the tangential line through posterior femoral condyles by superimposing transverse images through the apex of the intercondylar notch and the tibial tuberosity. TT-TG distance of more than 20 mm is nearly always associated with patellar instability, and is a measure for lateralization of tibial tuberosity. Values of 15–20 mm are considered borderline and distances less than 15 mm are considered normal.

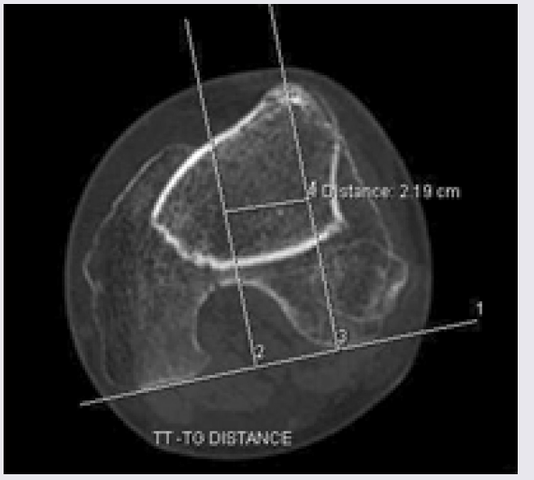

Fig. 2.18: Distance from the tibial tuberosity to the trochlear groove (TT-TG)

9. Femoral anteversion angle: Femoral anteversion refers to the orientation of the femoral neck in relation to the femoral condyles at the level of the knee. Femoral anteversion can be determined by measuring the angle formed between the long axis of the femoral neck and a line parallel to the dorsal aspect of the femoral condyles (posterior condylar axis, or PCA) on axial slices at MRI or CT. Femoral anteversion averages between 30–40° at birth, and between 8–14° in adults. An increased femoral anteversion is often seen in patients with developmental dysplasia of the hip. Moreover, it has been shown that abnormal femoral anteversion can contribute to the development of femoroacetabular impingement (FAI). Reduced femoral anteversion is associated with cam-type FAI.

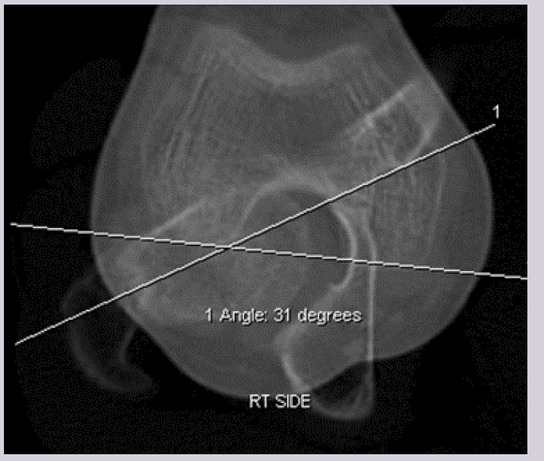

Fig. 2.19: Femoral anteversion angle

- No free fluid is seen in pouch of Douglas
- LMP: 16/02/2022

***Polycystic ovary*:** Multiple peripherally arranged follicles measuring about 3–4 mm in sizes noted in the bilateral ovaries with echogenic stroma. Right ovary volume 15 ml, left ovary volume 17 ml. No evidence of dominant follicle in both ovaries.

Ovarian simple cyst: A large abdominopelvic cystic mass with fluid attenuation measuring 14 × 12 × 15 cm. No obvious solid area, septations or calcifications are noted within. The mass appears to be intraperitoneal and seen to displace retroperitoneal structures, like pancreas and kidneys posteriorly. Right ovary could not be visualized separately. However, the left ovary is seen separate from the lesion (ORADS-3).

Torsion ovary: Right ovary appears enlarged measuring 4.5 × 3.8 cm with heteroechoic central stroma and peripherally displaced follicles, the ovary appears to be in minimal, the ovarian pedicle appears to be twisted with minimal flow through the pedicle, free fluid noted in pelvis. Left ovary appears normal.

Placenta accreta: placenta anterior with absence of placental myometral interface noted, the uterine wall being undistinguishable from the placenta, and the presence of multiple vascular intraplacental lacunae on Doppler ultrasound revealed an extensive vascularity along the anterior portion of the lower uterine segment and appears to extend up to and around the bladder.

***Ectopic pregnancy*:** No evidence of intrauterine gestational sac noted. endometrium appears thickened measuring 10 mm. Complex right adnexal cyst measuring 3 × 4.2 cm which on Doppler ultrasound shows ring of fire appearance—possibly right adnexal ectopic, suggested beta-HCG correlation.

IUGR: All fetal biometric parameters falling below the 3rd percentile, EFW-670 g, average gestation age 21 weeks, LMP gestation age 28 weeks. On Doppler ultrasound umbilical artery shows reversal of diastolic flow. Middle cerebral artery Doppler remained normal, cerebroplacental ratio <1—**features suggestive of Type-I (symmetric) intra-uterine growth restriction.**

Abdominal circumference and estimated fetal weight falls below the 3rd percentile with Doppler ultrasound umbilical artery shows pulsality index above 95 percentile and reversal of cerebroplacental ratio and oligohydramnios noted—**features suggestive of Type-II (asymmetric) intrauterine growth restriction.**

Ovarian malignancy: Large complex pelvic mass arising from the right adnexa measures about 11.5 × 13.4 × 10.9 cm. The mass compresses the uterus inferiorly and significant compression in the urinary bladder. The lesion shows multiple lobulations with solid, cystic and hemorrhagic component. Both ovaries are not made out separately. Features favour ovarian malignancy with bilateral iliac and paraaortic lymphadenopathy-ORADS 5.

Checklist: Side, component of lesion, invasion to bladder colorectal, pelvic side wall, anterioal abdominal wall, vessels, ascites (none/small/moderate/large), peritoneal metastases, lymphadenopathy (none/only below renal arteries/above and below renal arteries) in the region of internal iliac/external iliac/common iliac/retro-peritoneal/mesentric root/porta hepatis/splenic hilum. Any intra-abdominal organ, bone involvement. Look for any thoracic involvement in the form of parenchymal nodules, pleural effusion, lymphadenopathy.

Endometrial carcinoma: Irregular heteroechoic endometrial thickening measuring 2.5 × 4 cm showing myometrial invasion and minimal fluid collection, on

Table 2.22: Follicular study serial examination

Date	*Day*	*Right ovary*	*Left ovary*	*Endometrium*			*Prefollicular Flow*2*	*Ov art RI*3*		*Ov art PSV*4*		*POD*	*Remark*	*Sign*
				Width	*Type*	*Flow*1*		*Right*	*Left*	*Right*	*Left*			

*MSF-Multiple small follicles

1. No flow, ±Minimal sparse flow, +±Moderate flow,++±Good flow
2. 25% perifollicular flow—poor prognosis, 25–50% flow—intermediate prognosis, >50% perifollicular flow-good prognosis of conception, on the day of ovulation. However, complete peripheral follicular flow in preovulatory phase of cycle suggest poor outcome.
3. Ovarian artery RI<0.5—better prognosis (just before ovulation), >0.5 poor prognosis (in post-ovulation corpus luteal cyst.)
4. Ovarian artery PSV in cm/s—if >10 cm/sec good prognosis, favourable outcome
5. Endometrial thickness <8 mm is associated with poor pregnancy rates. Uterine artery S/D,RI and PI could not be used alone to predict endometrial receptivity.

Table 2.23: Types of endometrium with respect to normal menstrual cycle

Type	*Days*	*Endometrium description*	*Stages*	*Hormonal levels*
1	1–4	Hyperechoic with irregular borders	Menstruation	Low E2 and P
2	5–8	Linear and thin	Early proliferation	Low E2 and P
3	9–11	Leaf shaped, hypoechoic spongy layer with ill-defined basal layer	Mid proliferation	Increasing E2, ↑↑↑low P
4	12–14	Triple line appearance with well-defined basal layer (6–12 mm)	Late proliferation	E2 surge: E2, low ↑P
5	15–22	Echogenicity of spongy layer, gradual loss of middle inner layer	Early secretory	E2-minor peak, P to peak
6	23–28	Hyperechoic lumpy pattern with regular outline	Late secretory	↓E2, ↓P

Doppler study prominent feeding artery noted—possibly endometrial carcinoma suggested HPE correlation.

Checklist: Myometrial and serosal, presents of other benign lesion (adenomyosis, leiomyomas), cervical stroma, parametrial, bladder, rectal invasion. Comment about vagina and overies. Check for lymph nodes, ascites and peritoneal involvement.

Adenomyosis: Uterus appears bulky measuring 16 × 8 cm, with loss of endometrial and myometrial junction, junctional zone appears thickened measuring 15 mm with multiple small T2 hyperintense cystic areas noted.

***Endometriosis*:** Focal T2 dark well-defined lesion in the torus uterinus extending to the posterior uterine wall with areas of T1 hyperintensity—endometriosis.

***Checklist*:** Uterus size, junctional zone thickness, fibroids, cervix endometrium, ovaries (volume in ml) bladder, ureter, uterine ligaments, rectovaginal septum, anterior rectal wall, sigmoid colon, adjacent small bowl loops, lymph nodes and osseous structures.

Ca cervix: A large infiltrating soft tissue density mass lesion measuring 7.3 × 6.6 × 6.6 cm (CC × AP × TR) noted involving the cervix and lower uterine segment. The lesion shows moderate enhancement on contrast administration. Anteriorly, there is loss of fat plane between the mass and the posterior bladder wall with infiltration of the same. No significant intraluminal extension seen. Anteroinferiorly, mass infiltrates the anterior vaginal wall. Posterior vaginal wall is relatively normal. There is no infiltration of lower 1/3rd of vagina. There is significant parametrial invasion more on the left side with involvement of parametrial venous plexus on left side. There is infiltration of left distal ureter by the mass causing moderate hydroureteronephrosis. There is significant delay in excretion of contrast into the pelvicalyceal system. No pelvic side wall infiltration. Both obturator internus muscles are normal.There is no infiltration of the rectal wall seen. Multiple round soft tissue density deposits are noted along the surface of uterus. No hydrometra/pyometra (T3bN1M0).

Hydrosalpinx: Tubular-shaped anechoic structure with incomplete septation noted in the right adnexa, right ovary visualized separately, uterus and left ovary appears normal.

RADS—Reporting and Data System (Refer OSCE/core for detailed explanation)

TIRADS: A well-defined mixed hypoechoic solid and cystic lesion measuring 1.2 × 1.8 cm in size with the lesion appearing wider than taller and irregular margin containing a few areas of macro calcifications. No evidence of any extra thyroidal extension and punctate echogenic foci or peripheral rim calcifications seen—TIRADS 4 (4–6 points/moderately suspicious of malignancy). Suggested FNAC thyroid and follow-up.

LIRADS—reflect the probability of observation being a HCC and ranges from LR1 (definitely benign) to LR5 (definitely HCC).

Multiple well-defined new small (7 mm) nodular lesions are noted in the right hepatic lobe which are hypervascular on the arterial phase and mildly fades on portal venous phase, compared to background liver enhancement. There is no capsule around any lesion. There is no restricted diffusion and nodular liver surface is compatible with cirrhosis. There is no washout, no presence of an enhancing capsule (pseudocapsule) and no interval growth seen-features favours LI RADS III (intermediate probability for HCC). Suggested follow-up imaging in 3–6 months.

LIRADS can be used only in cirrhosis, Hep B, current/prior HCC. Not to use LIRADS in 18 years, cirrhosis due to congenital hepatic fibrosis, cirrhosis due to vascular disorders (Budd-Chiari, portal vein occlusion, diffuse nodular regenerative hyperplasia, cardiac congestion).

PIRADS: A well-defined lenticular shaped homogeneous, moderately T2 hypointense lesion with diffusion restriction noted in transition zone at the apex of the prostate gland noted measuring 9 mm (<1.5 cm in greatest dimension) with surrounding normal peripheral zone. There is no definite extra prostatic extension/invasive behaviour. The surrounding seminal vesicles appears normal. No pelvic nodes and bone involvement noted. Features favours PIRADS IV (high clinically significant cancer is likely to be present).

ORADS: An ill-defined large multi-locular abdomino pelvic cystic mass measuring 23.7 × 10.7 × 19.6 cm with no solid or papillary projections noted. Left ovary not visualised separately. A normal right ovary visualised separate from the mass. Uterus appears normal with endometrial thickness of 4 mm. There is no ascites and no evidence of visceral, peritoneal or nodal metastases noted. Features favour O RADS IV (intermediate risk of malignancy) (10% to <50%).

BIRADS: Refer to case 118 to 120.

An ill-defined isoechoic lesion measuring 3.9 × 3 cm with indistinct margin and posterior acoustic shadowing and architectural distortion of surrounding breast parenchymal tissues noted at 11–12 o'clock position in zone II of right breast. No axillary nodal involvement noted. Features favour BIRADS V (95% probability of malignancy). Suggested FNAC of right breast mass.

Lung RADS: Refer to case 105.

A well-defined ground-glass nodule with a mean diameter of 34 mm noted subpleural in location in inferior lingula segment of left lung with the nodule showing spiculated borders. There is double the increase in the size of the nodule compared to previous images taken 1 year back (16 mm in size). There are no enlarged regional lymph nodes noted. Features favour LUNG RADS IV-X (suspicious, >15% chance of malignancy).

Oncoimaging:

Renal cell carcinoma: FDG avid partially exophytic soft tissue density mass noted in the upper pole of the left kidney measuring ~59 × 62 × 83 mm (AP × TR × CC). The lesion shows heterogeneous enhancement on arterial phase (HU ~112) and washout on delayed phase (HU~ 59). Pelvicalyceal system is not infiltrated. Perinephric fat plane is not infiltrated. Preserved fat plane noted between the mass and spleen superiorly and descending colon anteriorly. Left renal vein is distended with thrombus, showing heterogeneous enhancement and mild FDG uptake. The thrombus is extending into the infrahepatic IVC. No extension noted into the suprahepatic IVC/right atrium. Left gonadal vein is distended. Dual left renal artery noted and the mass is predominantly supplied by the accessory branch. No other focal lesion noted in the left kidney. Right kidney appears normal. Multiple FDG avid enlarged paraaortic, pericaval and left retrocrural lymph nodes noted, largest measuring ~28 × 23 mm. Left adrenal gland appears normal. No evidence of pulmonary metastasis. No FDG avid skeletal lesions. (T3bN1M0)

Hilar cholangiocarcinoma: Ill-defined isodense soft tissue density lesion with mild FDG uptake is noted at the level of confluence of left and right hepatic ducts, measuring ~44 × 35 mm.The lesion is involving the entire length of common hepatic duct, hepatic duct confluence and left hepatic duct with extension up to the bifurcation. Moderate bilateral intrahepatic biliary radical dilatation noted. Common bile duct is not involved. Parenchymal atrophy noted in the left lobe. Proximal right and left branches of hepatic artery are encased by the lesion. Proper hepatic artery is normal. Left portal vein is infiltrated. Main portal vein and right branch are uninvolved. A few FDG avid periportal, portacaval, coeliac and left gastric lymph nodes noted, largest measuring ~18 × 12 mm. Enlarged left paracardiac lymph node is noted showing mild, FDG uptake, measuring ~12 × 10 mm. Multiple ill-defined hypodense lesions with mild FDG uptake noted in both lobes of liver, largest measuring ~23 × 18 mm in segment VII. **Features suggestive of biliary malignancy involving common hepatic duct, hepatic confluence, and left hepatic duct (Bismuth-Corlette-Type III b) with lymph nodal and hepatic metastases.**

Lymphoma–interim PET: Significant reduction in size and resolution of FDG uptake noted in left level III, level IV and supraclavicular lymph nodes noted, largest measuring ~ 17 × 9 mm, previously measured ~ 33 × 26 mm. Resolution of right hilar and subcarinal lymph nodes noted. Significant reduction in size with resolution of FDG uptake noted in bilateral subcentimetre axillary lymph nodes. Significant reduction in size and resolution of FDG uptake noted in paraaortic, bilateral common iliac and external iliac and inguinal lymph nodes noted, largest measuring ~21 × 7 mm, previously measured ~53 × 28 mm. Resolution of mesenteric lymph nodal mass noted. Mild reduction in size of the spleen noted with resolution of FDG avid hypodense lesions. Resolution of FDG uptake noted in both iliac bones with appearance of subtle sclerosis. **Deauville 2—complete metabolic response.**

Carcinoma lung—Follow-up PET-CT: Mild increase in size and FDG uptake noted in the soft tissue density mass with spiculated margins in apicoposterior segment of left upper lobe, measuring ~47 × 39 mm, previously

measured ~40 × 21 mm. Abrupt cut off of the segmental bronchus noted with distal collapse. The mass is infiltrating the mediastinal fat plane. Mild increase in size and FDG uptake noted in right hilar, aortopulmonary and right upper paratracheal lymph nodes, largest measuring ~29 × 17 mm, previously measured ~20 × 13 mm. Appearance of a few subpleural nodules in left lower lobe. Appearance of moderate left pleural effusion. Mild increase in size and FDG uptake noted in ill-defined hypodense lesions in both lobes of liver, largest measuring ~36 × 24 mm, previously measured ~23 × 21 mm. Appearance of FDG avid nodule in left adrenal gland measuring ~20 × 11 mm. Appearance of FDG avid lytic lesions noted in multiple vertebrae, multiple ribs, sternum and left acetabulum. D7 vertebral collapse noted causing moderate spinal canal narrowing. Appearance of nodular enhancement noted in left frontal and temporal lobes. No significant edema/mass effect noted. **Features are suggestive of disease progression (T2bN3M1c)**.

Neuroendocrine tumor–68Ga DOTANOC PET-CT; Jejuno-jejunal intussusception noted with a small submucosal lesion in the lead point showing significant 68Ga DOTANOC uptake, measuring ~39 × 14 mm. No evidence of bowel obstruction. Another tiny the mucosal nodular lesion with increased 68Ga DOTANOC uptake noted in the first part of the duodenum in the anterior wall, measuring ~9 × 7 mm. The nodules showing intense enhancement on arterial phase. No periserosal extension noted. Rest of the small bowel loops appear normal. Multiple enlarged 68Ga DOTANOC avid peripancreatic lymph nodes noted, largest measuring ~21 × 17 mm. No significant retroperitoneal lymphadenopathy. Multiple 68Ga DOTANOC avid lesions noted in both lobes of liver, more conspicuous on arterial phase, largest measuring ~21 × 23 mm. **Suggestive of neuroendocrine tumors in first part of the duodenum and the proximal jejunum with jejuno-jejunal intussusception, lymph nodal and hepatic metastases.**

Soft tissue sarcoma–right thigh: FDG avid heterogeneously enhancing mass noted in the anteromedial aspect of the right upper thigh in the muscular plane of right adductor longus and brevis muscles, measuring ~10.7 × 12.1 × 14.5 cm (AP × TR × CC). Enhancing thin capsule noted in the mass. Multiple nonenhancing cystic areas noted along the periphery of mass, predominantly near the inferior margin. Right adductor longus muscle is stretched and noted in the anterolateral aspect of the mass. Atrophic changes noted in the distal muscle fibres. Adductor brevis muscle is not separately visualized. Rest of the adductor compartment muscles appear normal. Neurovascular structures in the right adductor canal displaced anterolateraly. Branches of right profunda femoris are noted along the inferior margin of the mass. Right femur appears normal. No cortical erosion noted. No significant right ilio-inguinal lymphadenopathy. No pulmonary metastasis **(T3N0M0).**

Adenoid cystic carcinoma of sphenoid sinus: Heterogeneously enhancing lesion with mild FDG uptake noted in bilateral sphenoid sinuses, measuring ~68 × 42 × 35 mm. Anteriorly the lesion extending into bilateral posterior ethmoid air cells. Posteriorly the lesion is eroding the posterior wall of the sphenoid sinus. No extension noted into the prepontine cistern. Laterally, the lesion extending into the right pterygopalatine fossa. Further extension noted into the right foramen rotundum and inferior orbital fissure. Remodelling of posterior wall of the right maxillary sinus noted. Erosion and sclerosis noted in the right pterygoid bone. On the left side, the lesion encroaching the left sphenopalatine foramen with no further extension. Minimal erosion noted in the medial wall of the right orbit. No intraorbital extension noted. Superiorly erosion noted in the floor of the sella, planum sphenoidale and ethmoidale. The pituitary gland is displaced upwards. No intracranial extension. No obvious extension noted into the cavernous sinus. No significant cervical lymphadenopathy.

Right adrenal neuroblastoma: Large FDG avid lobulated heterodense mass with moderate enhancement noted in the right suprarenal region, measuring ~11.3 × 13.1 × 16.6 cm (AP × TR × CC). Right adrenal gland is not separately visualized. No calcification noted within the mass. Superiorly the mass is indenting the inferior surface of the liver with no evidence of infiltration. Superior extension noted up to the OG junction. Inferiorly the mass is displacing the right kidney. Inferior extension noted to the level of right common iliac vessels. Medially the mass is displacing the abdominal aorta anteriorly and extending across the midline. Inferior vena cava is encased and compressed by the mass. Laterally the mass abutting the right lateral chest wall. Anteriorly the mass is displacing the pancreas. Posteriorly the mass is extending up to the level of right D12–L1 neural foramen. However, no neural foraminal/intraspinal extension noted. Multiple FDG avid mesenteric lymph nodes noted, largest measuring ~18 × 14 mm. A few FDG avid lymph nodes noted in the paraaortic region, largest measuring ~12 × 12 mm. Moderate ascites noted. No metabolically active focal lesion noted in the liver. Multiple FDG avid bilateral upper paratracheal and prevascular lymph nodes noted, largest measuring ~13 × 11 mm. Multiple FDG avid left supraclavicular lymph nodes noted. No evidence of pulmonary metastasis. No FDG avid skeletal lesions noted. International Neuroblastoma Staging System Committee (INSS) system—**stage 4 disease**.